9-22-2023

EVALUATION OF DIGITAL TWIN APPROACHES FOR THERMAL MODELING AND ENERGY OPTIMIZATION FOR EXISTING BUILDINGS

Jason Bastie Muermann
Rowan University

EVALUATION OF DIGITAL TWIN APPROACHES FOR THERMAL MODELING AND ENERGY OPTIMIZATION FOR EXISTING BUILDINGS

by
Jason Bastie Muermann

A Thesis

Submitted to the
Department of Mechanical Engineering
College of Engineering
In partial fulfillment of the requirement
For the degree of
Master of Science in Mechanical Engineering
at
Rowan University
September 15, 2023

Thesis Chair: Francis M. Haas, Ph.D., Associate Professor, Department of Mechanical Engineering

Committee Members:
William T. Riddell, Ph.D., Associate Professor, Department of Civil & Environmental Engineering
Jess W. Everett, Ph.D., Professor, Department of Civil & Environmental Engineering and Department of Experiential Engineering Education

Dedications

I would like to dedicate this thesis to my mother, Amy Muermann, whose crucial role in my personal and academic development has been invaluable, especially during my challenging experiences as a foster child. Without her love and support through the adoption process, I would not have been able to reach my potential and become the person I am today. Her strong work ethic, determination, and drive have also been a source of inspiration to me. Her ability to balance a full-time job and a startup jewelry business has always amazed me, and I am grateful for the values of self-discipline and hard work that she has instilled in me.

This thesis is also dedicated to my grandfather, Dana Westcott, who was a significant influence on my decision to pursue an education in mechanical engineering. As a mechanical engineer himself, he instilled in me a deep respect for knowledge and encouraged me to enjoy life to the fullest. His passion for knowledge is reflected in his habit of reading encyclopedias and pursuing woodworking, and he was driven to take on challenging hiking expeditions, such as conquering the 46 peaks of the Adirondacks. I am deeply grateful for his inspiration and guidance, which has not only helped me grow professionally but also taught me to appreciate the value of life.

Acknowledgments

I would like to extend my sincere gratitude to my thesis committee members, Dr. Francis Haas, Dr. William Riddell, and Dr. Jess Everett, for their invaluable guidance and support throughout my research. Their expertise and communication have not only enhanced my writing skills but also contributed to my professional growth. The knowledge and skills I have gained will undoubtedly benefit me in my future endeavors.

I express my gratitude to the Construction and Facilities Management Office (CFMO) of the New Jersey Department of Military and Veterans Affairs (NJDMAVA) for their support in this research. The funding for this research was provided by NJDMAVA through collaborative projects with Rowan University's Sustainable Facilities Center (SFC).

I would like to acknowledge the significant contributions of Justin Costa to my thesis research. His efforts in arranging site visits and assisting with equipment setup for data collection were invaluable. Our collaboration played a crucial role in ensuring a successful data collection experience, and I am grateful for his support throughout my research journey.

I would like to extend my appreciation to the center's staff, particularly Kathleen Mullins and William Johnson, who have shown a keen interest in my professional growth and success as an engineer.

Finally, I want to express my heartfelt appreciation to Alyssa and Luna Condell for their understanding and patience during the demanding hours dedicated to my thesis research. Their support has been instrumental in my success throughout this challenging experience.

Abstract

Jason Bastie Muermann
EVALUATION OF DIGITAL TWIN APPROACHES FOR THERMAL MODELING AND ENERGY OPTIMIZATION FOR EXISTING BUILDINGS
2022-2023
Francis M. Haas, Ph.D.
Master of Science in Mechanical Engineering

Residential, commercial, and industrial building sectors in the United States were responsible for 42% of the nation's consumption of 100.2 quadrillion BTUs of energy in 2019 [1]. 80% of the nation's energy is sourced from fossil fuels, including coal, natural gas, and petroleum. Fossil fuels are known contributors to carbon emissions and climate change, making energy reduction vital. Consequently, New Jersey Department of Military and Veterans Affairs (NJDMAVA) is tasked with evaluating energy consumption and efficiency in all New Jersey Army National Guard (NJARNG) facilities, as mandated by TAG Policy Letter 18-5, Executive Order 13990, and the Energy Independence and Security Act of 2007. This research investigates three building energy consumption modeling (BEM) approaches for colder weather: eQUEST, degree-day modeling, and resistance-capacitance (RC) modeling. Each method has distinct advantages and limitations, but BEM holds promise in identifying cost-effective energy-saving measures, aligning with the goals of government entities like NJDMAVA. Specifically, eQUEST proves valuable for experienced users in energy modeling. Degree-day modeling excels at detecting operational shifts and benchmarking similar facilities. The RC model was able to accurately predict energy savings as a result of changes to thermostat settings.

Table of Contents

Table of Contents (Continued)

Table of Contents (Continued)

List of Figures

List of Figures (Continued)

Figure Page

List of Figures (Continued)

Figure Page

List of Tables

Table Page

Chapter 1

Introduction

Residential, commercial, and industrial building sectors in the United States were responsible for 42% of the nation's consumption of 100.2 quadrillion BTUs of energy in 2019 [1]. Domestic energy consumption for these applications is approximately 11% of the total global energy consumption [1, 2]. 80% of this energy is sourced from fossil fuels [1], such as natural gas, coal, and petroleum, which release carbon into the atmosphere and contribute to climate change [3]. Furthermore, forecasts suggest that reserves of natural gas and petroleum will be exhausted by 2066 and 2068, respectively [4]. Of additional concern is the United States Energy Information Administration's (EIA) projection that despite the effects of the coronavirus pandemic on reducing energy use in 2020-2022, the consumption of fossil fuels is expected to reach unprecedented levels in 2023 [5]. This trend is despite energy initiatives to reach national and global carbon neutrality by 2030 and 2050, respectively [6, 7]. Therefore, it is crucial to concentrate efforts on reducing the nation's energy consumption.

The Department of Defense (DOD) is the largest single agency consumer of energy in the United States federal government. The DOD spent $11.9 billion on energy, which represents approximately 76% of the federal government's energy expenditures and approximately 2% of the DoD's $619 billion budget during fiscal year 2017 [8]. Rowan University's Sustainable Facilities Center (SFC) provides annual building energy and water assessments to evaluate the energy consumption and efficiency of the New Jersey Department of Military and Veterans Affairs (NJDMAVA) and the New Jersey Army National Guard (NJARNG) facilities. This is a result of various federal and state

energy initiatives such as TAG Policy Letter 18-5, Executive Order 13990, and the Energy Independence and Security Act of 2007 [9-12]. NJARNG aims to reduce its energy use per square foot by 2.5% annually, for a total of 25% by the end of the fiscal year 2025, compared to the fiscal year 2015 baseline [9].

The United States Department of Energy (USDOE) has developed various building energy modeling (BEM) tools [13]. One such tool, eQUEST [14], is investigated in this study as a means of modeling changes to buildings and building operations to achieve this goal. However, BEM can be applied not only to NJARNG facilities, but also to other sectors, such as residential, commercial, industrial, and agricultural. BEM can be used to develop a digital twin of a building, allowing the potential effects of various energy-saving measures on the digital twin to be evaluated before spending time and money to implement on a real building.

1.2 Goals and Research Motivation

Rowan University's Sustainable Facilities Center (SFC) is aiding NJDMAVA with building energy and water assessments to reach the energy goals outlined in TAG Policy Letter 18-5, Executive Order 13990, and the Energy Independence and Security Act of 2007 [9-12]. A significant portion of the energy used in many buildings is related to space heating and cooling. Therefore, thermal modeling is an important aspect of overall BEM. This study submits that a digital twin developed through BEM is an effective tool for energy management and savings. The goal of this study is to identify advantages and tradeoffs related to using BEM approaches for the thermal modeling of a building, specifically to allow the appropriate choice of thermal modeling for NJDMAVA purposes. To reach this goal, the following objectives were identified:

1. Review literature to assess energy modeling techniques (white-box, black-box, and grey-box) and identify crucial parameters for model implementation.
2. Select the specific white-box, black-box, and grey-box models to investigate for this study.
3. Determine the effective methods for data collection that can be applied to each energy modeling approach.
4. Validate and verify the accuracy and reliability of the identified BEM techniques by comparing them to actual building performance data, such as historical utility bills during the heating season.
5. Identify the advantages and limitations of each energy modeling technique used in the research.
6. As proof of concept, use the models to predict the effect of temperature setbacks on energy use during the heating season.

1.3 Structure of Thesis

The basic principles of heat transfer and their application to buildings, as well as a literature review on the three broadly classified energy modeling techniques, are discussed in Chapter 2. The data collection and modeling techniques employed in this study are discussed in Chapter 3. The applications to two chosen study sites, Buildings A and B, are presented in Chapters 4 and 5, respectively. The results of the energy modeling techniques used in this study are also presented in these chapters. Conclusions of the research, including an analysis of the advantages and limitations of each energy modeling technique are discussed in Chapter 6.

Chapter 2

Literature Review

The fundamental heat transfer physics and their application to the management of buildings, as well as literature related to building energy modeling (BEM) techniques, are discussed in this chapter. This content informs the approach, results, and conclusions discussed in later chapters. The scope of the heat transfer discussion in this chapter is intended to address the objectives of this thesis.

2.1 Physics of Heat Transfer

The transfer of thermal energy, or heat, occurs when it moves from one area to another [15]. Heat will naturally flow from hotter regions to cooler regions, and terms like “loss” or “gain” are used to indicate the direction of heat transfer. Three fundamental mechanisms of heat transfer exist: conduction, convection, and radiation [16, 17]. These mechanisms are discussed in the following subsections.

2.1.1 Conduction

Conduction refers to the process of thermal energy transfer through a medium by direct contact between hot and cool matter [18]. This process is driven by temperature differences between relatively stationary bodies. The rate of heat conduction is dependent on temperature differences, as well as the size and material properties of the conducting matter. The material property that characterizes the rate of heat transfer by conduction that results from a thermal gradient in a material is thermal conductivity (k). Thermal conductivity is an intrinsic material property, as it is independent of size and shape. A material with low thermal conductivity is considered a thermal insulator. The reciprocal of thermal conductivity is thermal resistivity (r). Thermal resistance (R) is a measure of

resistance to heat flow per unit through a body and is defined as the ratio of the thermal conductivity of the body material to its thickness [19], as expressed in Equation 2.1. Figure 2.1 demonstrates the transfer of heat by conduction through a single layer of homogeneous material (where k is constant). For this illustration, it is assumed that side 1 is at a higher temperature than side 2.

$$R_{cond} = \frac{s}{k} \tag{2.1}$$

Where:

R_{cond} = thermal resistance to heat conduction per unit area, $m^2 \cdot K \cdot W^{-1}$

k = thermal conductivity of the material, $W \cdot m^{-1} \cdot K^{-1}$

s = thickness of the body, m

Figure 2.1

Conduction through a Single-Layered Solid Body

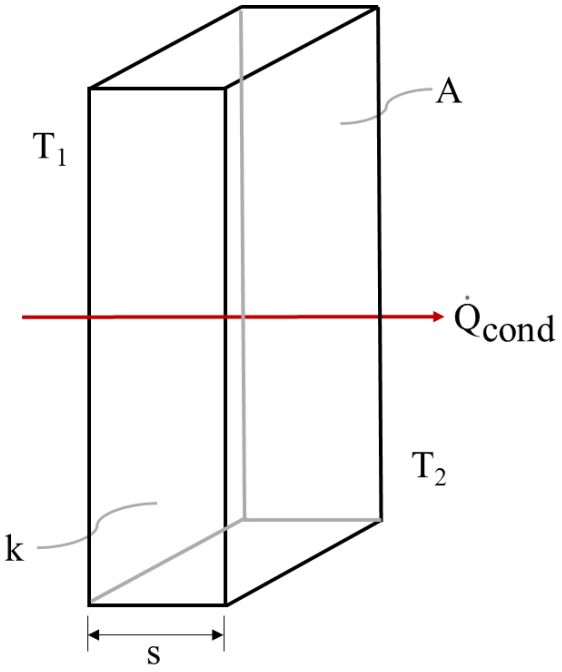

The rate of conductive heat transfer through a body is proportional to both the temperature difference between the two sides of the body and the area of the body and inversely proportional to its thickness, as described in Equation 2.2. The SI units indicated below are illustrative. The variables used here also admit other units (e.g., ft^2 and °F) without loss of generality. However, unit conversions may be required to harmonize other units in equations.

$$\dot{Q}_{cond} = \frac{A * (T_1 - T_2)}{R_{cond}} \tag{2.2}$$

Where:

$\dot{Q}_{cond}$ = rate of conductive heat energy transfer, W

A = cross-sectional area of the body perpendicular to the path of heat flow, m^2

T_1 = temperature on side 1 of the body, K

T_2 = temperature on side 2 of the body, K

2.1.2 Convection

Convection refers to the process of heat transfer that occurs in fluids (liquids or gases) when there is a temperature difference between regions of the fluid. As the fluid moves from a hot region to a cooler region, thermal energy is also transferred. In applications related to building science, convective heat transfer is divided into surface air convective heat transfer and infiltration or exfiltration (depending on the direction). Surface air convective heat transfer is discussed in the following subsection, whereas in/exfiltration is discussed in Section 2.2.2. The distinction between these cases is that in/exfiltration involves the mass of air entering or leaving a boundary of a control

volume, whereas surface air convective heat transfer does not involve mass crossing a boundary of a control volume.

The rate and direction (i.e., into or out of the surface) of surface air convective heat transfer depend on four main factors: the convective heat transfer coefficient (h), the cross-sectional heat-transfer area of the solid body perpendicular to heat flow, the surface solid-body temperature, and the flowing fluid temperature. The convective heat transfer coefficient (h), also known as the film coefficient, is a complicated function of the local flow velocity and flow geometry, fluid properties, and surface properties of the solid. Figure 2.2 illustrates the concept of convective heat transfer, where air at a temperature of T_f and velocity v flows past (perpendicular) a solid surface at temperature T_s. For surface heat convection, thermal resistance is defined as the reciprocal of the convective heat transfer coefficient, as expressed in Equation 2.3. Brackets are used to distinguish that h_{conv} is a function of v.

Figure 2.2

Surface Air Convection through a Solid Body

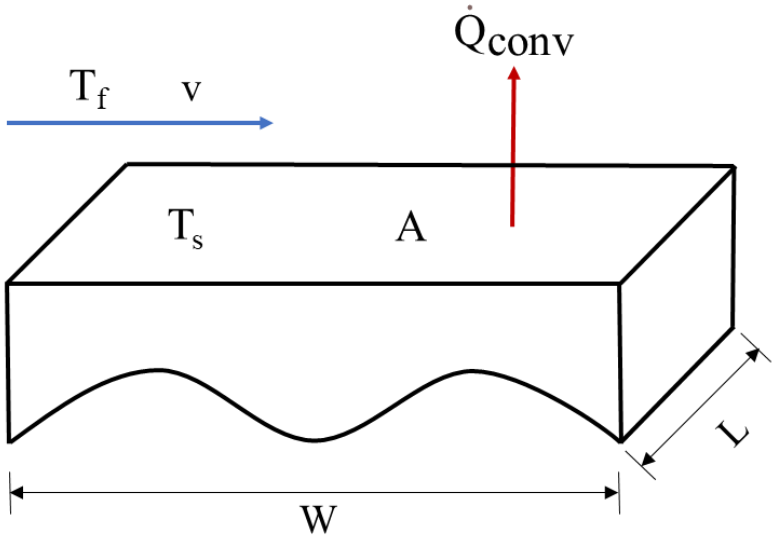

$$R_{conv} = \frac{1}{h_{conv}[v]} \tag{2.3}$$

Where:

R_{conv} = thermal resistance to surface heat convection, $m^2 \cdot K \cdot W^{-1}$

h_{conv} = convective heat transfer coefficient of the fluid, $W \cdot m^{-2} \cdot K^{-1}$

The formula for the rate of heat transfer by surface convection through an area determined by width W and length L and thermal resistance of R_{conv} is characterized by:

$$\dot{Q}_{conv} = \frac{A_s * (T_s - T_f)}{R_{conv}} \tag{2.4}$$

Where:

$\dot{Q}_{conv}$ = rate of surface convective heat transfer, W

A_s = cross-sectional area of the solid body perpendicular to heat flow, m^2

T_s = surface temperature of the solid body, K

T_f = temperature of the flowing fluid, K

2.1.3 Thermal Radiation

Thermal radiation is the transfer of heat that occurs through the emission and absorption of electromagnetic waves. When a body's surface temperature is above absolute zero (0 K), it will emit electromagnetic waves, that can transfer heat energy to another object without any physical contact or medium between them [20]. The terms "hot" and "cold" are used to describe the temperature of bodies involved in thermal radiation, without any loss of generality, and imply that the hot body has a temperature

that is higher than that of the cold body. The net result of thermal radiation will be heat transfer from a hot body to a cold body. This type of heat transfer occurs in all directions, as illustrated in Figure 2.3, and is proportional to the surface area of the radiating surface (hot body), the surface emissivity, and the temperature difference between the emitting surface and its surroundings (cold body), as expressed in Equation 2.5. For purposes of this discussion, this type of radiation is regarded as a form of heat generation. However, solar irradiance (not to be confused with solar radiation which is a measure of how much energy is emitted by the sun [21] is another form of heat generation, but more specifically for buildings, as it is the amount of solar radiation that reaches a specific area on Earth's surface per unit time [22], which is further discussed in Section 2.2.3.

Figure 2.3

Thermal Radiation by a Homogenous Hot Body

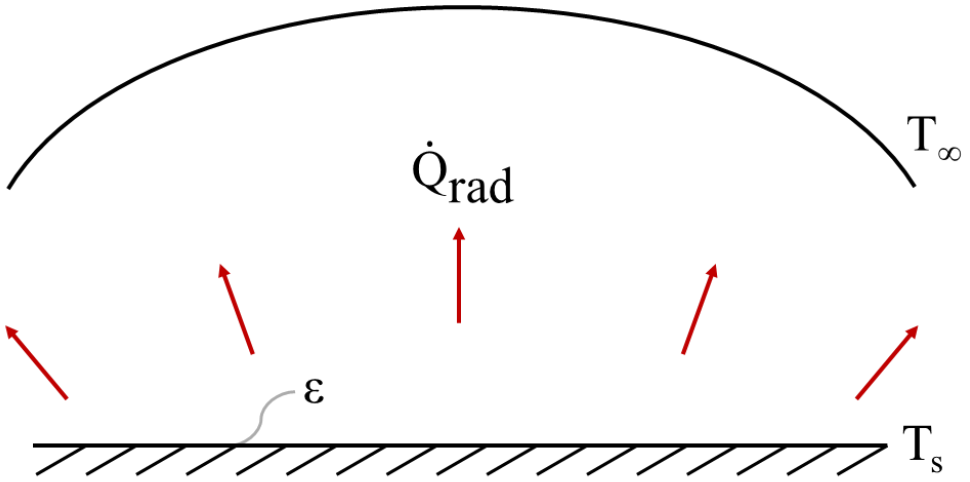

Note. This figure was adapted from [23]

$$\dot{Q}_{rad} = \varepsilon * \sigma * \left(T_s^4 - T_{surr}^4\right) * A_s \quad (2.5)$$

Where:

$\dot{Q}_{rad}$ = rate of heat transfer due to thermal radiation, W

ε = emissivity coefficient of the emitting surface (hot body)

σ = Stefan-Boltzmann constant, 5.67×10^{-8} $W \cdot m^{-2} \cdot K^{-4}$

T_s = surface temperature of the emitting surface (hot body), K

T_∞ = surface temperature of the surroundings (cold body), K

A_s = surface area of emitting surface (hot body), m^2

Surface emissivity is a measure of the efficiency with which a material can emit thermal radiation. It is defined as the ratio of the energy radiated by a material to that radiated by a blackbody at the same temperature conditions and can vary between 0 and 1 [24]. A blackbody is a hypothetical object that absorbs all incident radiation and emits radiation with maximum efficiency for a given temperature. The emissivity factor, ε, of a material is dependent on surface characteristics, such as color, texture, roughness, temperature, and composition, chemical properties, wavelength of the emitted radiation, atmospheric conditions, and angle of inclination [25]. Materials with rougher texture or darker color tend to exhibit higher emissivity factors, whereas those with smoother texture or lighter colors tend to exhibit lower emissivity factors. It is often difficult to estimate the emissivity of a material. However, based on experimental observations, various sources tabulate emissivity for various materials [26].

2.2 Heat Transfer in Buildings

Heat transfer in buildings affects the comfort, health, and safety of the building occupants, as well as the energy consumption and environmental impact of the building. The heat transfer mechanisms of conduction, convection, and radiation are all applicable to buildings, with heat loss (or gain) occurring through the building envelope through conduction and convection; through convection due to ventilation and air infiltration; and heat gain via solar radiation. The rate and direction of heat transfer are influenced by building-influenced conditions such as geometry and construction, and operation; as well as location-influenced conditions such as temperature, wind speed, and solar irradiance [27]. Simulating the physics of building heat transfer is essential for designing or analyzing the energy efficiency of buildings, as well as developing effective heating, ventilation, and air conditioning (HVAC) systems.

Heat transfer to or from a building will result in changes in the indoor temperature of a building. Thermal capacitance characterizes the amount of heat energy required to increase the temperature of the building [28]. In the context of a representative unit mass, thermal capacitance is characterized by the specific heat capacity. Thermal capacitance is an extensive thermal property because it depends on the size of a body, while specific heat capacity is an intensive material property because it is independent of the size and shape of the body.

2.2.1 Conductive and Surface Air Convective Heat Transfer in Buildings

Buildings typically experience combined conductive and convective heat loss to the surrounding environment through envelope components, such as exterior walls, windows, doors, floors, ceilings, and thermal bridges [27, 29, 30]. Heat transfer through

each component is driven by the temperature difference between the indoor and outdoor environments, through a combination of conductive heat transfer through multiple layers of the envelope component, as well as convection for both the internal and external walls. The conductive and convective thermal resistances can be treated as resistors in a series circuit to calculate the total thermal resistance of an envelope component. The thermal conductance (U) is the reciprocal of the thermal resistance (R) and can be calculated for a series of conductive and convective surfaces as expressed in Equation 2.6. This concept is illustrated in Figure 2.4, where a triple-layered building element is exposed to air movement inside (free) and air movement outside (forced) of the building. For this configuration, U_{tot} can be quantified by Equation 2.7.

$$U_{tot} = \frac{1}{\sum_{i=1}^{N} R_i} \tag{2.6}$$

Where:

U_{tot} = overall thermal conductance of building element, $W \cdot m^{-2} \cdot K^{-1}$

R_i = thermal resistance of N^{th} layer of building envelope component, $m^2 \cdot K \cdot W^{-1}$

Figure 2.4

Thermal Resistance Network for a Multi-Layered Building Structure

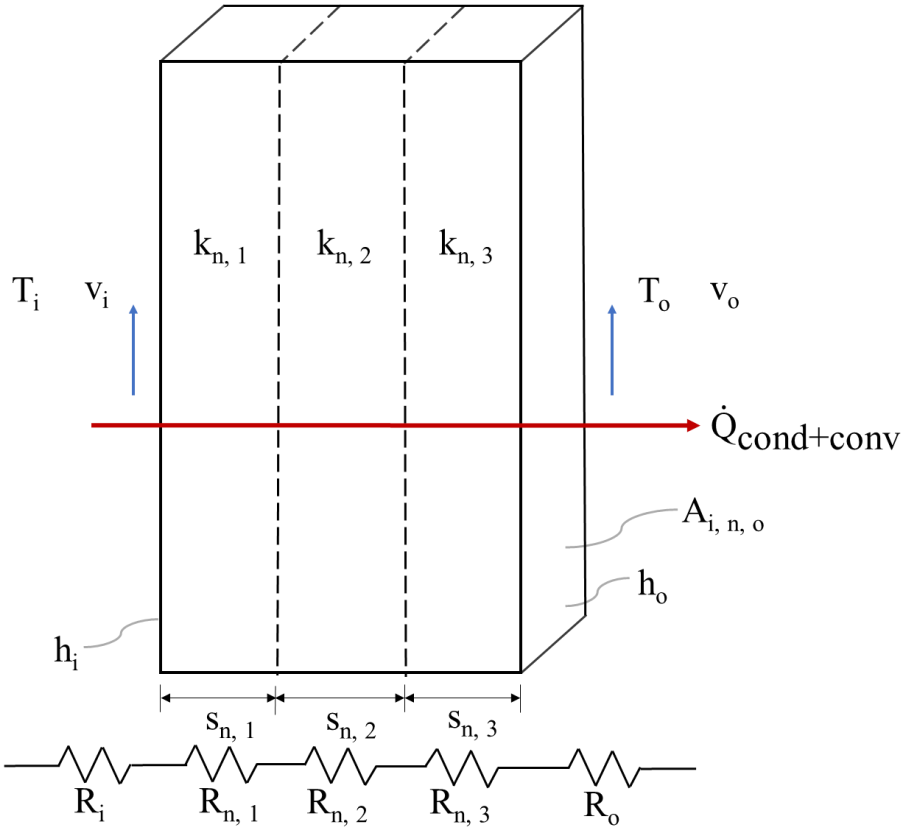

$$U_{tot} = \frac{1}{R_{conv,\,i} + R_{cond,\,1} + R_{cond,\,2} + R_{cond,\,3} + R_{conv,\,o}} \tag{2.7}$$

Where:

$R_{conv,\,i}$ = convective thermal resistance of the indoor environment, $K \cdot W^{-1}$

$R_{cond,\,1,\,2,\,3}$ = conductive thermal resistance of the element's three layers, $K \cdot W^{-1}$

$R_{conv,\,o}$ = convective thermal resistance of the outside environment, $K \cdot W^{-1}$

By introducing thermal conductance, U_{tot}, the formula for the rate of conductive and convective heat loss through a component can be quantified in Equation 2.8.

$$\dot{Q}_{cond+conv} = U_{tot} * A_{tot} * (T_1 - T_2) \quad (2.8)$$

Where:

$\dot{Q}_{cond+conv}$ = rate of conductive and convective heat loss, W

A_{tot} = total surface area of building element(s), m^2

T_1 = temperature of the indoor environment, K

T_2 = temperature of the outdoor environment, K

2.2.2 Air Exchange in Buildings

Two distinct forms of air exchange occur in buildings: ventilation and air infiltration/exfiltration. Ventilation involves intentionally moving indoor air in and out of the building to maintain adequate indoor air quality (IAQ), while air infiltration refers to the unintentional flow of outdoor air into the building through gaps in the building envelope, such as foundation cracks and poorly sealed doors and windows [31]. These concepts are illustrated in Figure 2.5, where outdoor air at temperature T_o enters the building and mixes with indoor air at temperature T_i, and then is replaced by a new mass of outdoor air at temperature T_o. In theory, thermal energy is exchanged across the building envelope control volume. The following sections of this thesis will discuss each of these air exchange mechanisms separately, starting with ventilation and followed by air infiltration.

Figure 2.5

Mass Flow Balance from Air Exchange

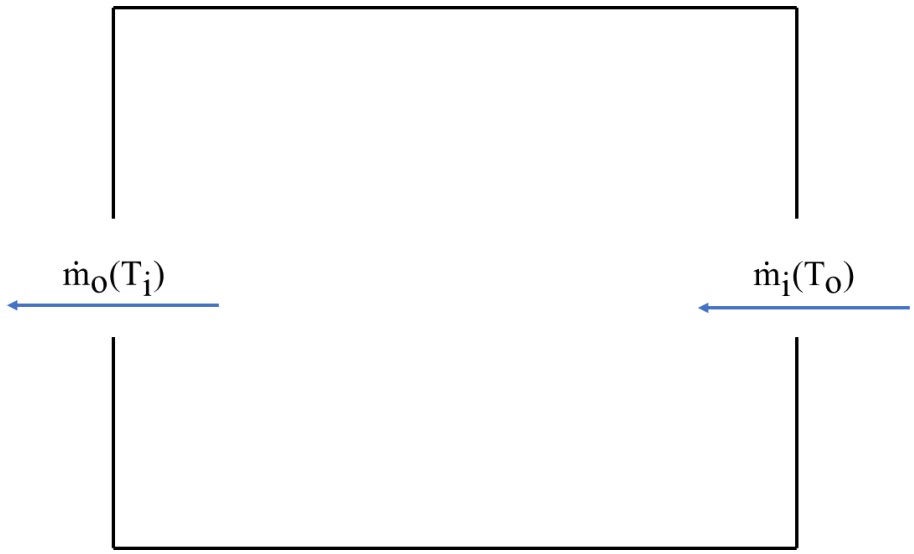

Heat loss from these processes can be calculated using the concept of thermal capacitance (C). The thermal capacitance of a body can be described by Equation 2.9.

$$C_{th} = \rho * V * c_p \quad (2.9)$$

Where:

C_{th} = thermal capacitance of the substance, $J \cdot K^{-1}$

ρ = density of the substance, $kg \cdot m^{-3}$

c_p = specific heat capacity of the substance, $J \cdot kg^{-1} \cdot K^{-1}$

V = volume of the substance, m^3

m = total mass of substance, kg

2.2.2.1 Ventilation in Buildings. Indoor air quality (IAQ) is important, and ventilation plays a crucial role in maintaining appropriate indoor temperature and humidity levels, removing pollutants, replenishing oxygen levels, reducing moisture and mold growth, and preventing the spread of airborne pathogens and unpleasant odors [32]. Ventilation requirements vary depending on the building's characteristics (e.g., types of rooms, etc.) and the building's modes of operation (e.g., number of occupants, frequency of use, etc.). Different areas in a building may require different ventilation rates due to varying moisture and occupancy levels. For example, bathrooms and offices may require different ventilation levels. If ventilation is inadequate, building occupants may experience mild to severe health effects. The American Society of Heating, Refrigerating, and Air-Conditioning Engineers (ASHRAE) has developed guidelines for air quality in buildings. These guidelines are outlined in ASHRAE 62.2 [33].

The effectiveness of ventilation in buildings can be estimated in several different ways: the air exchange method (AER), tracer gas method, and computational fluid dynamics (CFD) method [34-36]. The AER estimates the number of air changes per hour (ACH) to determine how many times the air within a space is replaced with fresh outdoor air by considering the airflow rate and the volume of the space [34]. The tracer gas method involves introducing a known quantity of a tracer gas (usually an inert gas like sulfur hexafluoride or helium) into a space and then measuring the concentration of that gas over time [35]. CFD modeling is a computational simulation technique that uses mathematical models to analyze airflow patterns, temperature distribution, and pollutant dispersion to estimate ventilation rates in buildings [36]. Regardless of the method used to quantify $\dot{m}_{vent}$, the resulting heat loss can be calculated using Equation 2.10.

$$\dot{Q}_{vent} = \dot{m}_{vent} * c_{p,\,air} * (T_i - T_o) \quad (2.10)$$

Where:

$\dot{Q}_{vent}$ = rate of heat loss due to ventilation, W

$\dot{m}_{vent}$ = mass flow rate from ventilation, $kg \cdot s^{-1}$

$c_{p,air}$ = specific heat capacity of the indoor air, $J \cdot kg^{-1} \cdot K^{-1}$

2.2.2.2 Infiltration in Buildings. Air infiltration occurs when outdoor air unintentionally flows into a building through gaps in its envelope, and is generally considered detrimental to building energy efficiency as it results in significant heat loss. Inefficient construction or maintenance of a building can result in significant heat loss caused by air infiltration, typically occurring through gaps or openings around the exterior windows and doors. Continuous air barriers are installed in buildings to reduce the rate of infiltration in buildings [37]. Various materials can serve as effective continuous air barriers, including rigid options like foam board insulation, drywall, plywood, or OSB, as well as flexible choices such as house wrap and fluid-applied membranes (e.g., liquid membranes applied using brushes, rollers, or sprayers) [37]. Notably, a study conducted by the National Institute of Standards and Technology (NIST) in 2005 demonstrated that reducing air infiltration through a continuous air barrier could yield energy savings of up to 36% [38].

The rate of infiltration in buildings can be estimated in several different ways: the blower door test, smoke pencil test, and infrared (IR) thermography. The blower door test involves the sealing of all openings in a building's envelope (doors, windows, vents,

etcetera) and then using a calibrated fan to depressurize the building [39], specifically through doorways. The rate of air infiltration can be calculated from the airflow rate required to maintain a constant pressure differential. The smoke pencil test involves using a smoke pencil or smoke stick to visually identify areas where air is leaking into or out of the building [40]. The non-toxic smoke is drawn to areas where there is air movement, indicating the presence of leaks. IR thermography involves using an IR camera to detect temperature differences on the surface of the building envelope [40]. Areas of air leakage can be identified by the presence of cooler or warmer spots where air is infiltrating or escaping. In cases where the aforementioned tests are not available, it is possible to estimate the rate of heat loss due to infiltration in buildings by utilizing algebraic equations. These equations will be discussed in the following sections.

Several factors influence the rate and direction of heat loss due to infiltration in buildings. However, for the purposes of this research using the crack-method [18], seven specific factors are considered: the density of the indoor air, the heat capacity of the indoor air, the length of the crack, the indoor temperature, the outdoor temperature, the wind speed, and the type and condition of the exterior window or door. It is important to understand that the terms “infiltration” and “infiltration rate” are both used in this thesis, but are not interchangeable. Infiltration is the term used to describe the rate of volumetric airflow per unit length of crack as outdoor air enters the building. Table 2.1 provides tabulated values for infiltration, considering factors such as the type and condition of the exterior window and door, as well as wind speeds.

Table 2.1

Infiltration in Cracks of Windows and Doors

Type of Window	Remarks	Wind Velocity, mph					
		5	10	15	20	25	30
Double Hung Wood Sash Windows (Unlocked)	Around frame in masonry wall - not calked	3	8	14	20	27	35
	Around frame in masonry wall - calked	1	2	3	4	5	6
	Around frame in wood frame construction	2	6	11	17	23	30
	Average window, non-weatherstripped, 1/16" crack and 3/64" clearance. Includes wood frame leakage	7	21	39	59	80	104
	Ditto, weatherstripped	4	13	24	36	49	63
	Poorly fitted window, non-weatherstripped, 3/32" crack and 3/32" clearance. Includes wood frame leakage	27	69	111	154	199	249
	Ditto, weatherstripped	6	19	34	51	71	92
Double Hung Metal Windows	Non-weatherstripped, locked	20	45	71	96	125	154
	Non-weatherstripped, unlocked	20	47	74	104	137	170
	Weatherstripped, unlocked	6	19	32	46	60	76
Rolled Section Steel Sash Windows	Industrial pivoted, 1/16" crack	52	108	176	244	304	372
	Architectural projected, 1/32" crack	15	36	62	86	112	139
	Architectural projected, 3/64" crack	0.2	52	88	116	152	182
	Residential casement, 1/64" crack	6	18	33	47	60	74
	Residential casement, 1/32" crack	14	32	52	76	100	128
	Heavy casement section, projected, 1/64" crack	3	10	18	26	36	48
	Heavy casement section, projected, 1/32" crack	8	24	38	54	72	92
Hollow Metal, Vertically Pivoted Window	General	30	88	145	186	221	242
Doors	Well fitted	27	69	110	154	199	-
	Poorly fitted	54	138	220	308	398	-

Note. The units provided in this figure are in $ft^3 \cdot hr^{-1} \cdot ft^{-1}$. This table has been adapted from [18].

Infiltration rate refers to the volume of air per unit time that enters the building and is typically measured in cubic feet per hour. Assuming that the length of the crack is evenly distributed across all four sides of exterior windows or doors, and considering only heat loss, the infiltration rate can be quantified in Equation 2.11.

$$\text{I.R.} = \left(\frac{L_c * I}{2}\right)_{\text{windows}} + \left(\frac{L_c * I}{2}\right)_{\text{doors}} \tag{2.11}$$

Where:

I.R. = infiltration rate, $m^3 \cdot s^{-1}$

L_c = length of crack, m

I = infiltration, given in Table 2.1, $m^3 \cdot s^{-1} \cdot m^{-1}$

The heat loss rate due to infiltration can be calculated using Equation 2.12.

$$\dot{Q}_{inf} = \rho_{air} * c_{p,\,air} * (T_i - T_o) * \text{I.R.} \tag{2.12}$$

Where:

$\dot{Q}_{inf}$ = heat loss rate due to ventilation, W

ρ_{air} = density of the indoor air, $kg \cdot m^{-3}$

T_i = temperature of the indoor environment, K

T_o = temperature of the outdoor environment, K

2.2.3 Solar Radiation in Buildings

Solar radiation is electromagnetic radiation that originates from the Sun [41]. Humans perceive solar radiation as sunlight. When this radiation passes through Earth's

atmosphere, it can be reflected, transmitted, or absorbed by various elements such as air molecules, water vapor, dust, pollutants, forest fires, and debris from volcanoes [41]. This interference results in diffuse solar radiation, whereas the solar radiation that directly reaches the Earth's surface is called direct beam solar radiation, which may also be reflected, transmitted, or absorbed by buildings. Solar radiation will increase the temperature of a body it strikes, making solar radiation a source of heat gain and solar cool loss. Hence, building design and operations can be tailored to manage the impact of solar radiation to maximize its benefits during the winter months while minimizing its negative effects during the summer months.

Scientists have measured the downward longwave and shortwave radiation that reaches Earth's surface for specific locations at different times of the year [41]. Downward longwave radiation plays a crucial role in regulating the Earth's overall temperature and maintaining a habitual climate since it is trapped by greenhouse gases in the atmosphere [42]. In contrast, downward shortwave radiation, which includes diffuse and direct radiation, is primarily responsible for heating the Earth's surface during the day since it is not trapped by greenhouse gases in the atmosphere in the same way as longwave radiation [42, 43].

The National Renewable Energy Laboratory (NREL) has developed solar resource maps [44] and the National Aeronautics and Space Administration (NASA) has developed the Prediction of Worldwide Energy Resource (POWER) Data Access Viewer [45], which are tools for analyzing the available global energy resources. Specifically, the POWER Data Access Viewer provides a wide range of meteorological data sets, including hourly, daily, and monthly averages for variables such as temperature,

precipitation, wind speed, and solar radiation (in $kWh \cdot m^{-2} \cdot day^{-1}$). However, estimating the amount of longwave and shortwave radiation that is reflected, transmitted, or absorbed by a building is challenging. The absorbed solar radiation adds heat to the building and affects the indoor temperature [46]. The amount of solar radiation absorbed by a building depends on several factors, including the wall's structural characteristics and orientation, the heat-transfer coefficient of the outer surface of the south wall (e.g., U-factor of windows), the radiation intensity, shading or glazing technology, and the outdoor temperature, among other natural environmental conditions [47, 48]. Additionally, the inclusion of inclination and reflection angles illustrated in Figure 2.6, like those for photovoltaic systems, significantly influence how much solar radiation is reflected, transmitted, or absorbed by a building. The rate of solar-induced heat generation in a building is denoted, $\dot{Q}_{rad}$.

Figure 2.6

Solar Radiation in Buildings

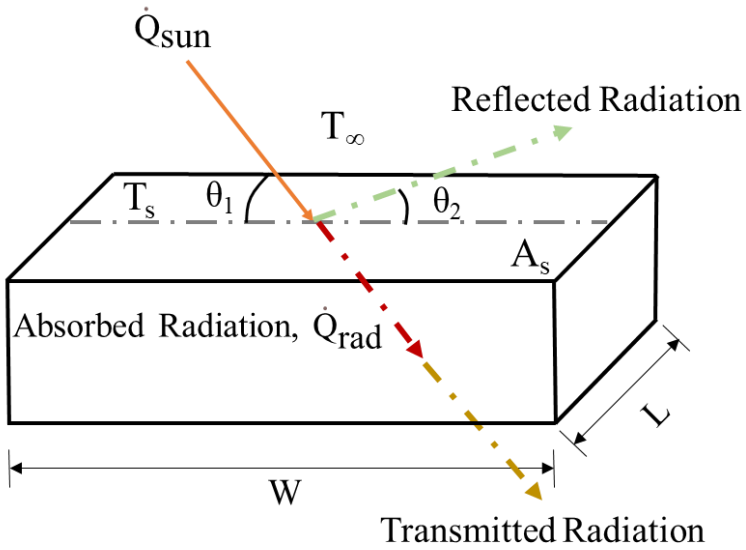

Note. This figure has been adapted from [49].

2.2.4 Heat Generation in Buildings

The primary source of heat generation within buildings is the heating component of the heating, ventilation, and air conditioning (HVAC) system. This system is responsible for regulating indoor temperature, humidity, and air quality to ensure occupant comfort and safety [50]. It is important to note that objects within the building also contribute to heat generation through internal thermal radiation, as discussed in Section 2.1.3. Additionally, electrical equipment in the building generates heat due to electrical resistance. However, this study does not delve further into these specific aspects. The rate of heat generation by HVAC systems in a building is denoted, $\dot{Q}_{HVAC}$.

2.2.5 Net Heat Flow in Buildings

The net heat flow rate in a building is described by Equation 2.13. If the outcome of the calculation yields a negative value, it indicates that the building is gaining heat. Conversely, if the value is positive, it implies that the building is losing heat.

$$\dot{Q}_{net} = \dot{Q}_{cond+conv} + \dot{Q}_{vent} + \dot{Q}_{inf} - \dot{Q}_{rad} - \dot{Q}_{HVAC} \tag{2.13}$$

2.2.6 Degree-Days

A degree-day (DD) is a climatic design indicator that is widely used in the design and operation of energy-efficient buildings [51]. DDs are calculated by comparing the average outdoor temperature to a specific base temperature. The calculation involves subtracting the base temperature, which is defined as the mean outdoor temperature above or below which the heating or cooling system in a building is not needed to maintain comfortable indoor conditions for occupants [52, 53], from the average outdoor temperature for a given period. Therefore, the units of a degree-day (day-°F) are not

constrained by a specific duration of time, as it can be applied to different periods, most commonly days, months, and years.

The deviation between the outdoor temperature and the base temperature introduces the concept of heating degree-days (HDDs) and cooling degree-days (CDDs), which quantitatively measure the demand placed on the heating and cooling systems, respectively [54]. In other words, HDDs accumulate when the outdoor temperature is lower than the base temperature. Contrarily, CDDs accumulate when the outdoor temperature is above the base temperature. During an unspecified duration when the outdoor temperature fluctuates above or below the base temperature, the calculation of HDDs and CDDs involves determining the integral of the temperature differences between the outdoor and base temperatures. This process is visually demonstrated in Figure 2.7 and mathematically represented by Equations 2.14 and 2.15, respectively. Subsequent sections will explore relevant literature on degree-days and their application as a black-box modeling technique.

Figure 2.7

Calculation of Heating Degree-Days

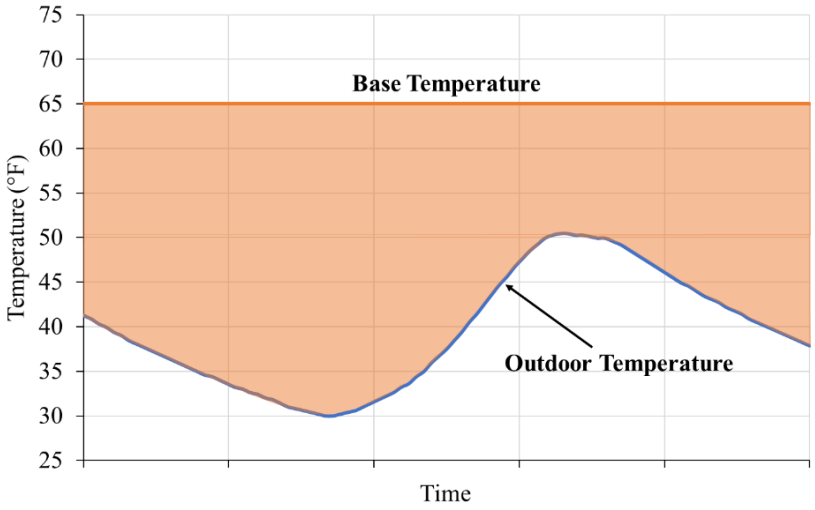

$$HDD = \int (\Delta T * dt) = \left[\int_{t_1}^{t_2} \max\left(0, T_{base,\ heating} - T_{out}\right) * dt \right] \tag{2.14}$$

$$CDD = \int (\Delta T * dt) = \left[\int_{t_1}^{t_2} \max\left(0, T_{out} - T_{base,\ cooling}\right) * dt \right] \tag{2.15}$$

The heat transfer that occurs during a finite time can be written as Equation 2.16. Equation 2.17 demonstrates the relationship between degree-days and the temperature disparities between the outdoor and base temperatures.

$$\Delta Q = \int \dot{Q} * dt$$
$$= \left\{ \left(\sum UA + \dot{m}_{vent} * c_{p,\ air} + \rho_{air} * c_{p,\ air} * I.R \right) * \int \Delta T * dt \right\} - \Delta Q_{rad} - \Delta Q_{HVAC} \tag{2.16}$$

$$DD = \int \Delta T * dt \tag{2.17}$$

2.3 Building Energy Modeling

Building energy modeling (BEM) has been developed as a multipurpose tool in the architecture, engineering, and construction (AEC) industries to simulate the energy performance of buildings. This is because of an increased awareness of several environmental and technological issues [55]. BEM can also be used to satisfy energy code compliances, and to qualify for green certifications, tax credit and utility incentives for buildings [56]. The results produced by BEM can be utilized to identify and justify energy conservation measures (ECMs) and energy efficiency measures (EEMs), which refer to advocations for new or retrofit designs that decrease energy consumption [57]. The BEM approaches explored in this study can be classified into three classifications: white-box, black-box, and grey-box modeling [58], based upon the degree to which physical processes are directly accounted for in a model. These classifications are summarized in Figure 2.8. Relevant literature for each classification of modeling will be discussed in the following subsections.

Figure 2.8

Different Classifications of Energy Models

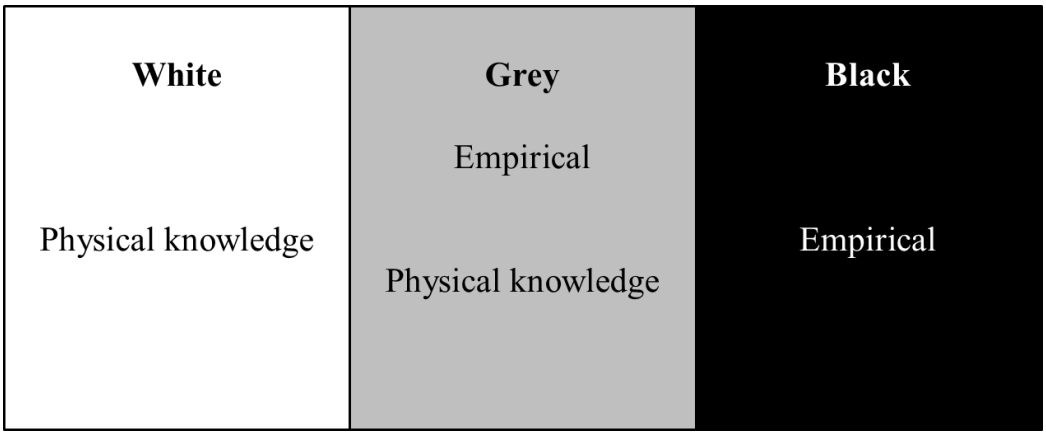

Note. This figure has been adapted from [59].

2.3.1 White-Box Modeling

White-box energy models are based on physical, thermodynamic, and other first-principal properties of the analyzed system. These models are often based on complex dynamic equations that describe the development of the building's heat balance [60]. Literature has promoted the utilization of white-box modeling for buildings, but these classifications of models require extensive knowledge of building characteristics such as configuration and orientation, as illustrated in Figure 2.9. Lack of perfect information regarding the building at the level of detail accounted for in a white-box model can limit the effectiveness of these models [59, 60].

Figure 2.9

User Inputs for White-Box Models

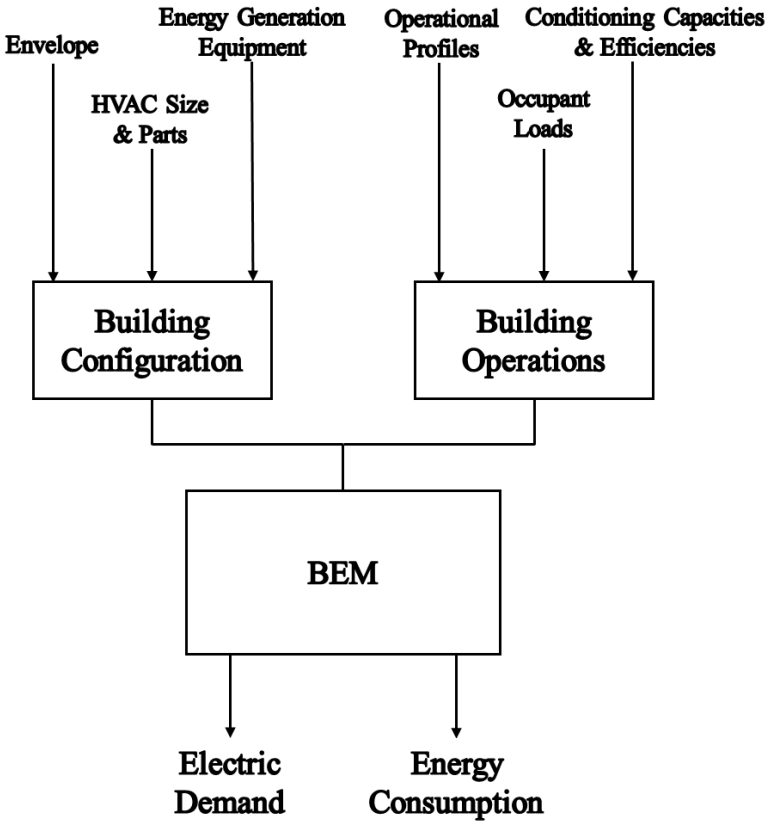

Energy modelers have utilized several different computer-based white-box models such as Autodesk Green Building Studio (GSB) [61], EnergyPlus [62], eQUEST [14], and TRNSYS [63]. Autodesk GSB is a flexible cloud-based service that requires an Autodesk Revit [64] model as the basis for energy analysis [61]. EnergyPlus is the newest generation console-based simulation tool developed and maintained by the USDOE. It represents a new generation of building energy simulation programs based on BLAST and DOE-2 that can predict sub hourly building energy consumption. eQUEST is an energy simulation tool that uses the DOE-2 computational engine to model a building's annual energy consumption [14]. It was first developed by the USDOE in 1998 but is now maintained by James J. Hirsch & Associates (JJH) in collaboration with the National Renewable Energy Laboratory (NREL). TRNSYS is a flexible graphics-based software used to simulate the behavior of transient systems in buildings [63]. It was developed by the University of Wisconsin's Solar Energy Laboratory.

Studies have compared the simulation results for building energy consumption of eQUEST to other white-box modeling techniques such as Autodesk GSB, EnergyPlus, and TRNSYS. [65] identified that eQUEST was much easier to use and less time consuming than Autodesk GSB when investigating the potential energy savings created by the removal and replacement of all original windows and exterior non-structural infill brick panels coupled with the installation of supplementary insulation materials between the new brick panels and interior concrete masonry unit (CMU) walls of several residence halls constructed in 1965. Rallapalli [66] discovered that EnergyPlus produced more accurate results, especially for more complex building systems, but was more time consuming than eQUEST. Dutta and Samanta [67] found that TRNSYS produced more

accurate results than eQUEST when parameterizing five different types of single and double-glazed windows of a building located in a tropical climate. The root-mean-square error (RMSE) and relative error (RE) were measured. The RMSE for the TRNSYS and eQUEST models were 2.1% and 12.5%, respectively. The RE for the TRNSYS and eQUEST models were 19.6% and 18.0%, respectively. Similarly, Dutta and Samanta [67] found that eQUEST produced results more quickly. Since the buildings analyzed in this study have simpler orientations, configurations, and HVAC systems, eQUEST was explored as the focal white-box approach.

Energy modelers have trusted the computational capability of eQUEST to simulate several different building components. eQUEST models are tuned by comparison to historical utility bills to measure their predictive accuracy. Song et al. [68] utilized eQUEST to analyze the effect of varying indoor personnel density, lighting power, summer design temperature, and summer air supply for a university library. Zerroug and Dzelzitis [69] used eQUEST to study the effect of varying insulation and thickness on the heat space energy consumption. Zafaranchi [70] utilized eQUEST to measure its predictive accuracy and investigate several passive energy retrofit measures (ERMs) such as thermal conductance of windows and shading devices, thermal insulation, surface area the exposed building envelope, window-to-wall ratio (WWR), and lighting systems for a building in Istanbul, Turkey. Ki et al. [71] used eQUEST to model the energy consumption of an office building. Teamah et al. [72] used eQUEST to evaluate the effect of several building parameters such as increased building air tightness, wall and roof insulation and an upgraded boiler for a commercial building located in Ottawa, Canada. Muhammad and Karinka [73] implemented eQUEST to simulate the

energy efficiency and human comfort (indoor air temperature and relative humidity) in a laboratory space located in Witte, India. The model showed that increasing the insulation thickness and installing low emissivity glass windows would provide comfortable conditions for occupants. Xing et al. [74] was used eQUEST to analyze the effect of changing several building components such as the schedule of internal loads, occupancy rate, and coefficient of performance (COP) of the chillers. The study identified that the COP of the chillers had the greatest effect, and its magnitude was confirmed by post-implementation. Leung and Ge [75] was used to measure the effect of indoor temperature setbacks to ensure thermal comfort and save energy for a single-family residence located in Bolton, Ontario. The model identified that reduced temperature setpoints could save 10% of energy consumption and that there was a 2% in energy consumption for every temperature setpoint decrease of 1 °C during the unoccupied hours of the building. Khan and Baqi [76] utilized eQUEST to model the effect of varying wall and roof building components for a full-scale cubical model. The study found that the building with brick walls and a FCIP insulated roof had a reduced annual energy consumption (2,383 kWh/year) as compared to the model with brick masonry walls and a concrete roof (10,190 kWh/year).

2.3.2 Black-Box Modeling

Black-box models are statistical-based models that do not require the same level of physiological information as white-box models [60]. These models can provide users meaningful results of the analyzed system when there is limited knowledge of the system, but require large and informative datasets [77, 78]. Black-box models achieve this by establishing a functional relationship (either

simple linear [79], multiple linear [80, 81], or non-linear [51, 79, 82] between the system's independent (input) and dependent (output) variables [83]. Several researchers have used the degree-day method as a black-box approach to analyze climate zoning [51, 84-87], climate change [88, 89], and building energy consumption, which will be discussed further in following sections.

Safa et al. [90] developed a degree-day model to predict the energy consumption of a cold storage building in New Zealand based on the amount of fruit stored (mainly kiwi and avocado) and other environmental factors using multiple linear regression (MLR) analysis. The study observed that the facility's weekly energy usage can be predicted by outside temperature and the number of store pallets. Moletsane et al. [91] used a degree-day model to estimate the relationship between degree-days (both HDDs and CDDs) between energy consumption (both electricity and natural gas) for two smart residential homes (labeled as Home B and C) with a central air conditioning and a gas-powered heating system located in western Massachusetts. The study identified a good correlation between Home B's CDDs and Home C's HDD when compared to their respective energy consumptions. However, a bad correlations was found between Home B's HDD and Home C's CDD when compared to their respective energy consumptions. Nishimwe and Reiter [92] investigated how the heat consumption of existing residential, tertiary, and industrial buildings located in southern Belgium would be influenced by future climate changes (HDDs) to aid decision-makers to set up future efficient energy management strategies. The HDDs and energy consumption (in TWh) for residential and tertiary buildings

were predicted between 2012 and 2050 while industrial buildings were modeled between 2016 and 2050. The study predicted that the predicted increase in temperature (between +0.17 °C and +2.28 °C) would result in a significant decrease in HDD (between -8.93% and -17.23%) and heat consumption (between -6.70% and -15.83%) for each building type. Terés-Zubiaga et al. [93] utilized a degree-day model to justify the installation of individual metering and charging (IMC) for a multi-family building located in northern Spain. The study established a strong direct correlation between HDDs and domestic hot water (DMC) heating consumption. In addition, other literature have stated that the calculated HDDs and CDDs can be used to estimate the fuel or cooling or heating energy requirement for buildings [94].

2.3.3 Grey-Box Modeling

Grey-box models are based on combinations of simplified physical information as used by white-box models, and statistical information, as used by black-box models. Resistance-capacitance (RC) modeling is a common grey-box approach that researchers have used to model behavior such as: waterflooding [95-101], heat exchangers [102-104], phase change storage tanks [105], oil recovery techniques [95, 106], and building energy performance models.

RC models for the energy consumption of buildings are the focus of this study. Resistive (R) and capacitive (C) parameters are selected by statistically processing measured data (e.g., indoor temperature, outdoor temperature, electricity consumption, and natural gas consumption) instead of extensive building information often required by white-box models. Stochastic first

differential equations are used to measure the fundamental heat transfer mechanisms in buildings, which were discussed earlier in this chapter.

Li et al. [107] utilized a two-resistance, 1 capacitance (2R1C) model to measure the performance of a pipe-embedded concrete radiant floor system. Numerical and experimental data were used to validate the model, showing that RC models can be beneficial for the design and optimal control of floor systems. Jeon et al. [108] developed a 7R5C model in conjunction with a weather prediction tool using forecasting information provided by local Korean weather centers to estimate the building load and demand for predictive control. The model was compared to a reference model developed in EnergyPlus and results (indoor air temperature within 0.5 °C) indicated high model accuracy. Kämpf and Robinson [109] used a two-node RC model to predict the indoor temperature of a building and measure the impact of an Urban Heat Island (UHI) effect on the building's energy consumption. The study concluded that the two-node RC model provided accurate results for both single- and multi-zone buildings when compared to the model created in ESP-r [110].

Chapter 3

Data Collection and Analytical Techniques

3.1 Context of the Chapter

The analytical techniques and data collection used in this study are presented in this chapter. Various classifications of data, including electric and natural gas consumptions, heating (HDDs) and cooling degree-days (CDDs), and indoor and outdoor temperatures, were gathered for the three classified modeling approaches employed in this study: white-box, black-box, and grey-box. Representatives of these classifications are eQUEST, degree-day, and resistance-capacitance (RC) modeling, respectively. However, it is important to note that not all classifications of data were collected for each modeling approach.

3.1 Analytical Techniques for Building Thermal Performance

The classification of data each analytical technique requires is discussed in the following subsections. Because of the classification of each analytical technique, each requires different levels of information.

3.2.1 eQUEST Modeling

eQUEST is a white-box modeling approach that utilizes DOE-2 software to simulate the annual energy consumption of a building [14]. There are three distinct user interfaces available for energy analysis: the Schematic Design (SD) Wizard, Design Development (DD), and Energy Efficiency Measure (EEM) Wizard. Both the SD and DD Wizards necessitate a comprehensive understanding of the building, as evidenced by the various user screens involved. One such screen, displayed in Figure 3.1 as the *HVAC Systems Definition* screen in eQUEST's DD Wizard, offers an overview of the numerous parameters essential

to creating an accurate model. The EEM Wizard enables users to assess the financial and economic savings resulting from various energy conservation measures (ECMs) or efficiency measures (EEMs).

Figure 3.1

HVAC System Definition Screen in eQUEST Model

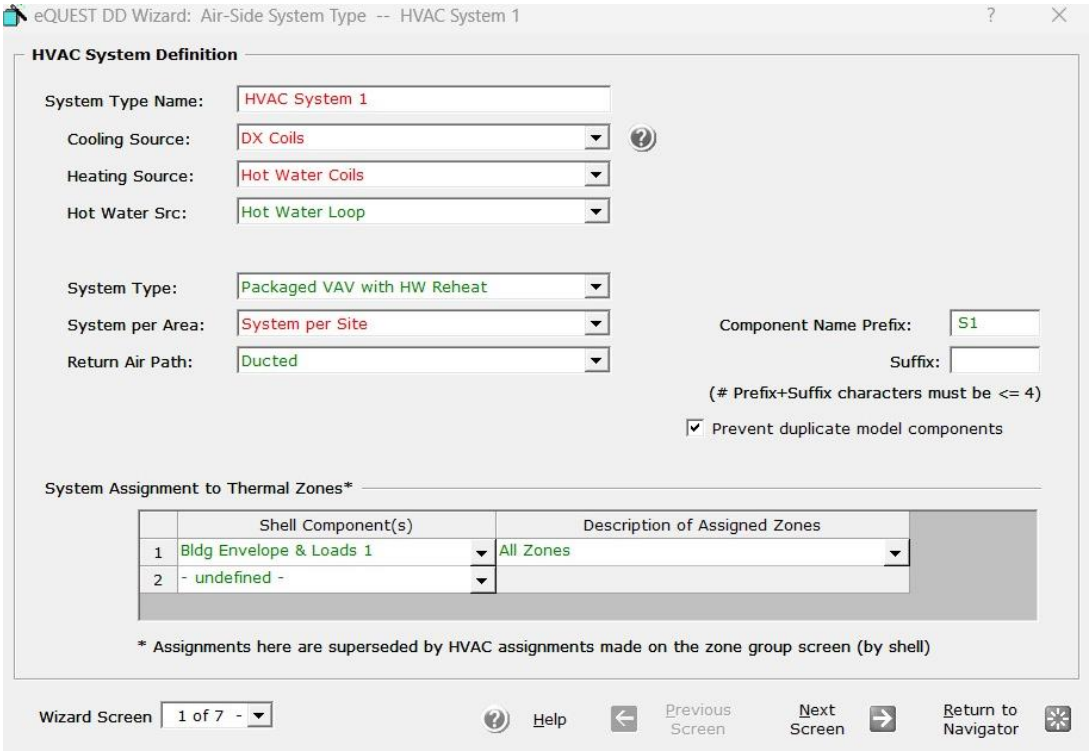

Note. Green text represents default values while red text indicates altered values.

Obtaining building configuration and operation details is crucial for this model, and these can be acquired on-site visits and consultations with building managers and users, including the building operator (specifically, the armorer for NJDMAVA facilities). Additionally, building plans, containing structural, mechanical, electrical, plumbing layouts, HVAC schedules, and other pertinent

documentation prove highly valuable in determining the various parameters within eQUEST. Once these variables are established, eQUEST can simulate monthly energy consumption, categorized by utility type, for a specified year. This simulation utilizes an online database that considers the building's location and historical weather data.

3.2.2 Degree-Day Modeling

Degree-day modeling is a black-box modeling approach that aims to establish linear relationships between degree-days and energy consumption. This method can help identify changes in building operation (e.g., boiler maintenance shut off, low-occupancy, etcetera) and estimate the energy consumption of a building if a linear relationship has been established. A degree-day model can be created once historical heating (HDDs) and cooling degree-days (CDDs), along with historical energy consumption (electric and natural gas consumption in this study) have been collected.

3.2.3 Resistance-Capacitance Modeling

Resistance-capacitance (RC) modeling is a grey-box modeling approach used to simulate the heat flow within a building caused by temperature differences between distinct spaces. Heat transfer within a building depends on the thermal characteristics of both the interior and exterior components of the building. The physical properties of the building's envelope, as well as the indoor and outdoor temperatures, and the electric and natural gas consumption (if applicable) are all important information for developing RC models.

3.3 Data Collection Techniques

In this research, various data collection techniques were employed to gather different types of data. Specifically, historical electric and natural gas consumption data were acquired through two distinct methods and utilized in the eQUEST, degree-day, and RC models. The degree-day model incorporated historical HDDs and CDDs, while the RC model incorporated indoor and outdoor temperatures.

3.3.1 Electric and Natural Gas Consumption

Historical electric and natural gas consumption data for the degree-day model were acquired by UtilityAnalytics, which is AvidXchange's automated consumption analysis and payment procession solution [111]. Specifically, monthly electric and natural gas utility bills were transferred and organized into a spreadsheet. Although this information was not required to create an eQUEST model, it was used to assess the accuracy of the model.

Historical electric and natural gas consumption data were also collected using the Wyze Cam v3 [112], which is a home security camera that was used to monitor real-time electric and natural gas consumption indicated by local meter displays. This equipment is an alternative to smart meter technology, which was unavailable at the site. The Wyze Cam v3 has Wi-Fi connectivity. However, this feature was disabled to follow NJDMAVA security protocols [113]. Instead, continuous 1-minute silent videos were saved to a local 128 GB microSD storage card. For manual harvesting of meter readings, subsequent trial tests confirmed that this setup had sufficient storage to perform intended operations with accuracy

that was sufficient to create an RC model. Representative camera footage for both utility meters during the day and night is shown in Figure 3.2.

Figure 3.2

Wyze Camera Footage for Electricity (top) and Natural Gas (bottom) meters. Daytime images are on the left, nighttime images are on the right at Building B.

Note. Utility information presented has been redacted as per sponsor order [113].

3.3.2 Heating and Cooling Degree-Days

An online software tool called Degreedays.net [114] was used to generate heating (HDDs) and cooling degree-days (CDDs) for the degree-day model. This tool, developed by BizEE, calculates degree-days using temperature data from weather stations across the world [114]. To use the software, users select a local weather station identification number, base temperature, time breakdown, and

period length. The generated HDDs and CDDs can be downloaded in units of Celsius (°C) or Fahrenheit (°F) in a spreadsheet.

3.3.3 Indoor and Outdoor Temperature

Two distinct temperature sensors manufactured by Onset [115] were utilized to obtain indoor and outdoor temperatures. The HOBO UA2300 measures and records indoor temperatures between -4 °F and 158 °F with an accuracy of ± 0.95 °F. This device also has outdoor and water temperature capabilities that were not used in this study. The HOBO MX2304 is suitable for outdoor applications, and measures and records temperatures between -40 °F and 158 °F with an accuracy of ± 0.36 °F. HOBO MX2304 sensors were used to record outdoor temperatures for this project. Because of its outdoor application, an Onset RS3-B solar radiation shield was installed on the MX2304 sensors to avoid solar heating aberrations. Both devices have a battery life of over 300 days with a sampling rate of 15 minutes. Initial tests verified that the data recorded by each temperature sensor had errors of less than 1 °F, and was deemed sufficient to provide the basis for an RC model.

Chapter 4

Data Collection and Energy Modeling Analysis of Building A

4.1 Context of the Chapter

RC modeling was implemented for Building A to demonstrate the feasibility and mechanics of this analytical technique. The effect of solar radiation on Building A, which was not a major focus of this study, was investigated in this case study. Once the model's fundamental heat transfer physics were confirmed, three energy conservation measures (ECMs) to measure the potential reduction in energy consumption, energy cost, and carbon emissions were implemented virtually in different case studies, which are discussed further in the following subsections. Other analytical techniques that were previously introduced in Chapter 2, such as eQUEST and degree-day modeling, were not explored since Building A is unconditioned and does not have an independent electricity metering system.

4.2 Facility Description of Building A

Building A is an unconditioned two-story shed located in southern New Jersey. This building is comprised of a lower space and an upper space. The upper level can be reached through an access hatch in the ceiling of the lower space. Both areas are primarily used for storage with some daily activity during the weekends (Friday through Sunday). Additional building details are provided in Appendix A.

4.3 Resistance-Capacitance Model for Building A

Figure 4.1 shows the location of three HOBO UA2300 indoor temperature sensors. Two sensors (A and C) were deployed on the ground level of Building A,

while a third temperature sensor (B) was deployed on the upper level. Additionally, an MX2304 outdoor temperature with a solar radiation shield (A0) was placed on the north side of the building. Following the deployment of the temperature sensors, the upper level of the building was closed off from the ground floor. Fifteen-minute interval data collection commenced on March 2, 2022, at 1:30 PM, and concluded on March 11, 2022, at 9:00 AM.

Figure 4.1

Location of Indoor and Outdoor Temperature Sensors at Building A

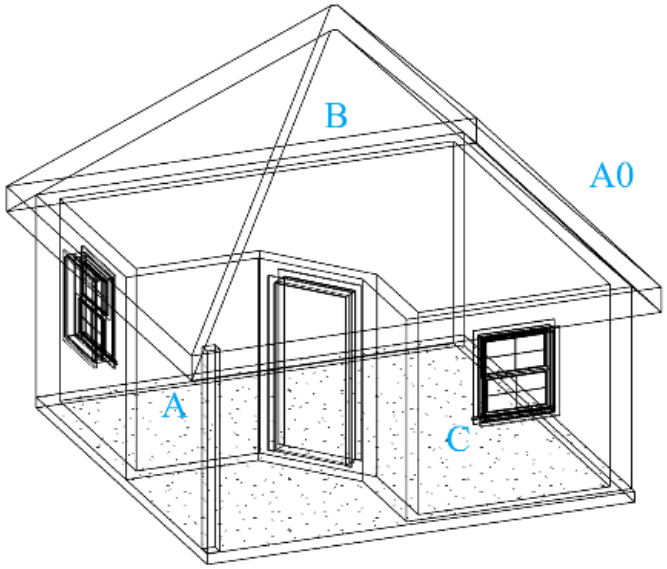

The temperature data collected suggests that Building A can be represented by two capacitive elements connected to each other and the outside and the ground by four resistive elements (4R2C). The capacitive elements are indicated in blue, while the resistive elements are represented by red single arrows indicating positive heat transfer or heat loss, as depicted in Figure 4.2. Heat is transferred via conduction, convection, air

infiltration, and solar radiation through the ceiling, roof, floor, and walls of the building. However, solar radiation was not a major focus of this study.

Figure 4.2

Heat-Balance Model of Building A

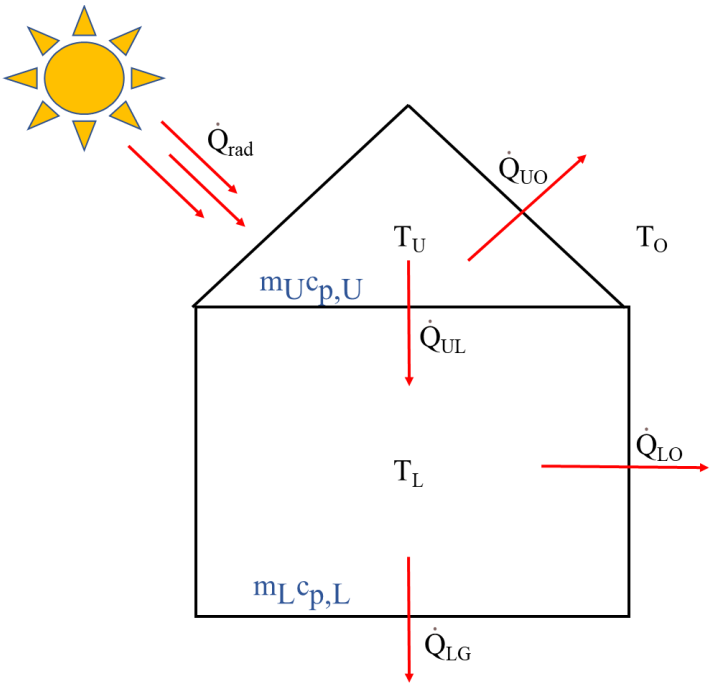

Non-transient heat transfer conditions were assumed in the 4R2C model. The ground temperature, T_G, was considered to be constant at 55 °F, while the outdoor temperature was regarded as a time-dependent variable. The thermal resistances of the ceiling, roof, floor, and exterior walls were designated as R_C, R_R, R_F, and R_{EW}, respectively, and were selected based on the climate zone 4 insulation standards established by the United States Department of Energy [116]. These standards are presented in Table 4.1. The thermal capacitances of the lower and upper sections of Building A were determined using Equation 2.10, assuming the specific heat capacity, c_p

and density, ρ of dry air at sea level and at typical indoor conditions (68 °F – 77 °F) [18]. The temperature of the upper and lower sections of Building A are the unknown values that the model solves for.

Table 4.1

USDOE Recommended Insulation Standards for Climate Zone 4

Building Component	Symbol	Insulation Standard ($ft^2 \cdot °F \cdot hr \cdot Btu^{-1}$)
Uninsulated Attic	R_C & R_R	R-60 (10.54)
Uninsulated Floor	R_F	R-19 (3.34)
Uninsulated Wood Frame Wall	R_{IW} & R_{EW}	R-25 (10.56)

Note: Metric units (K/W) are in parentheses

Table 4.2

Capacitive Properties of Building A

Building Area	c_p (J/kg·°K)	ρ (kg/m^3)	V (m^3)	C_{th} (J/K)
Lower Area	1,012	1.2	63	77,184
Upper Area	1,012	1.2	21	25,728

The thermal time constant is a measure of the time taken for the thermal mass (or indoor air and other building contents, in this study) to respond to change in the surrounding temperature [117]. It represents the time required for a thermal mass to attain 63.2% of the total difference between its initial and final body temperature when subjected to a step function change in temperature under zero power conditions [117]. Equation 4.1 [118] expresses the thermal time constant of a body.

$$\tau = \frac{\rho * V * c_p}{h * A} \quad (4.1)$$

Where:

τ = thermal time constant of the body, seconds

ρ = density of the body, $kg \cdot m^{-3}$

V = volume of the body, m^3

c_p = specific heat capacity of the body, $J \cdot kg^{-1} \cdot K^{-1}$

h = convective heat transfer coefficient of the body, $W \cdot m^{-2} \cdot K^{-1}$

A = surface area of the body, m^2

In Table 4.3, a summary of the variables utilized in determining the thermal time constant for the lower section of Building A is presented. The resulting thermal time constant was 761.16 seconds, or 12.68 minutes. A thermal time constant that is lower than the data collection and analysis interval indicates that the subsequent model (discussed in the following subsections) can have a significant numerical artifact appearing as oscillating "noise". A smaller data collection interval (~5 minutes) should be used instead for future work.

Table 4.3

Thermal Variables of the Lower Area of Building A

Building Area	c_p ($J \cdot kg^{-1} \cdot K^{-1}$)	ρ ($kg \cdot m^{-3}$)	V (m^3)	h ($W \cdot m^{-2} \cdot K^{-1}$)	A (m^2)
Lower Area	1,012	1.2	84.73	1	115.54

4.3.1 Case Study A1

The initial case study focuses on how solar radiation impacts the lower and upper areas of Building A. To simplify the model, the study used daily All Sky Surface Shortwave Downward irradiance (ALLSKY_SFC_SW_DWN) data obtained from NASA's POWER Data Access Viewer [45]. Adjustment factors were derived from this data, and Table 4.4 presents these factors. These factors were then applied to the lower are upper areas of Building A.

Table 4.4

All-Sky Surface Downward Shortwave Solar Radiation Data for Building A

Solar Radiation ($kWh \cdot m^{-2} \cdot day^{-1}$)	Lower Factor	Upper Factor
0 - 1	1.001	1.005
1 - 2	1.002	1.006
2 - 3	1.003	1.007
3 - 4	1.004	1.024
4 - 5	1.006	1.050
>5	1.007	1.055

In Figure 4.3, the graphical representation shows only a minor difference (<5 K) between the modeled temperature and actual temperature of the lower area of Building A when solar radiation was not considered. However, in Figure 4.4, there was a significant difference between the modeled temperature and actual temperature of the upper area of Building A when solar radiation was not considered. This outcome was expected,

indicating that solar radiation had a more significant impact on the upper area of Building A than the lower area.

Figure 4.3

Case Study A1 Results for the Lower Area of Building A

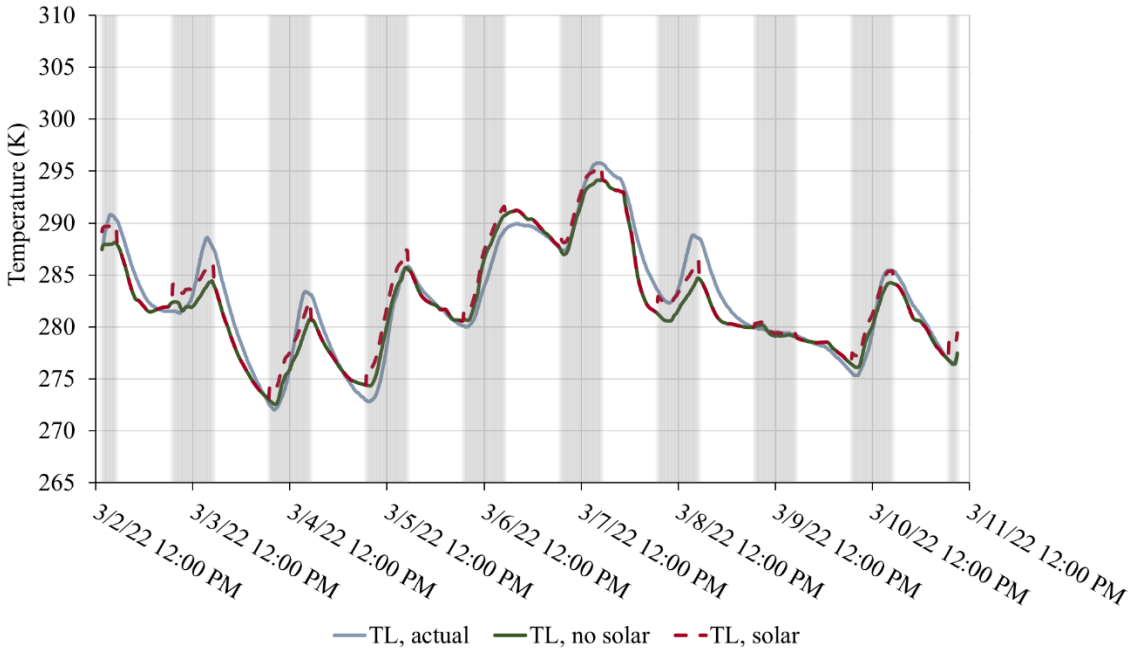

Figure 4.4

Case Study A1 Results for the Upper Area of Building A

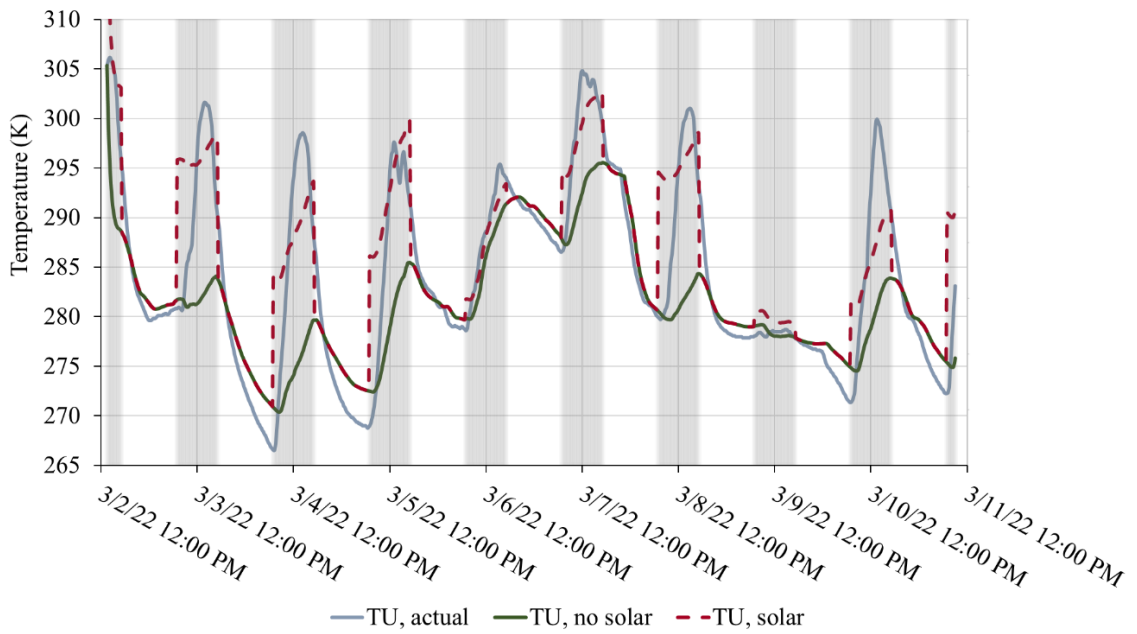

Note. Shaded regions represent operating hours of Building A (7 AM – 5 PM)

The conclusion based on the graphical representation was validated using the statistical measure of root mean square error (RMSE). In this study, RMSE is calculated by taking the square root of the average of the squared differences between the predicted and actual temperatures, as demonstrated in Equation 4.2. For the lower area, the RMSE between the measurements and model predictions was 1.7 K when solar radiation was not included, and it remained essentially the same when solar radiation was added to the model. In contrast, the RMSE for the model of the upper area was 6.8 K when solar radiation was not considered, but it decreased to 4.7 K when solar radiation was included. The RMSE values determined for Building A are similar in magnitude to ASHRAE limits on temperature drifts and ramps (e.g., a monotonic change of 2.2 K over 1 hour) [119]. While, in detail, the ASHRAE limits and the RMSE values cannot be directly

compared in a mathematical sense, both measure departures from the baseline temperature are comparable in this general sense. Table 4.5 provides a summary of these findings, which suggest that solar radiation impacted the upper area of Building A more significantly than the lower area. Nonetheless, since the study primarily focuses on the lower area of the building, the inclusion of solar radiation in the subsequent case studies was deemed unnecessary.

$$RMSE = \sqrt{\frac{\sum_{i=1}^{N} (T_{predicted} - T_{actual})^2}{N}} \tag{4.2}$$

Where:

RMSE = root mean square error of dataset, K

$T_{predicted}$ = predicted (or forecasted) temperature, K

T_{actual} = actual (or measured) temperature, K

N = sample size

Table 4.5

RMSE for Case Study A1

T_L without Solar RMSE	T_L with Solar RMSE	T_U without Solar RMSE	T_U with Solar RMSE
1.646	1.654	6.814	4.739

4.3.2 Case Study A2

The following case study investigates the impact of varying sizes of heating equipment (100 W, 400 W, 900 W) on the indoor environment of the lower area of Building A. The model in this case study utilizes the assumptions discussed in Section

4.3.1 and disregards the influence of solar radiation. The heaters modeled are activated when the indoor temperature of the lower section of Building A falls below 60 °F, which is the regulated occupied heating setpoint established by the United States Army for an occupied warehouse building [120]. Conversely, the heaters are turned off once the setpoint is reached. This is a simple model for control, but it was considered sufficient for this particular study. The findings of the preliminary research are demonstrated in Figure 4.5, while Figure 4.6 is used to mitigate the numerical noise in Figure 4.5.

Figure 4.5

Case Study A2 Results

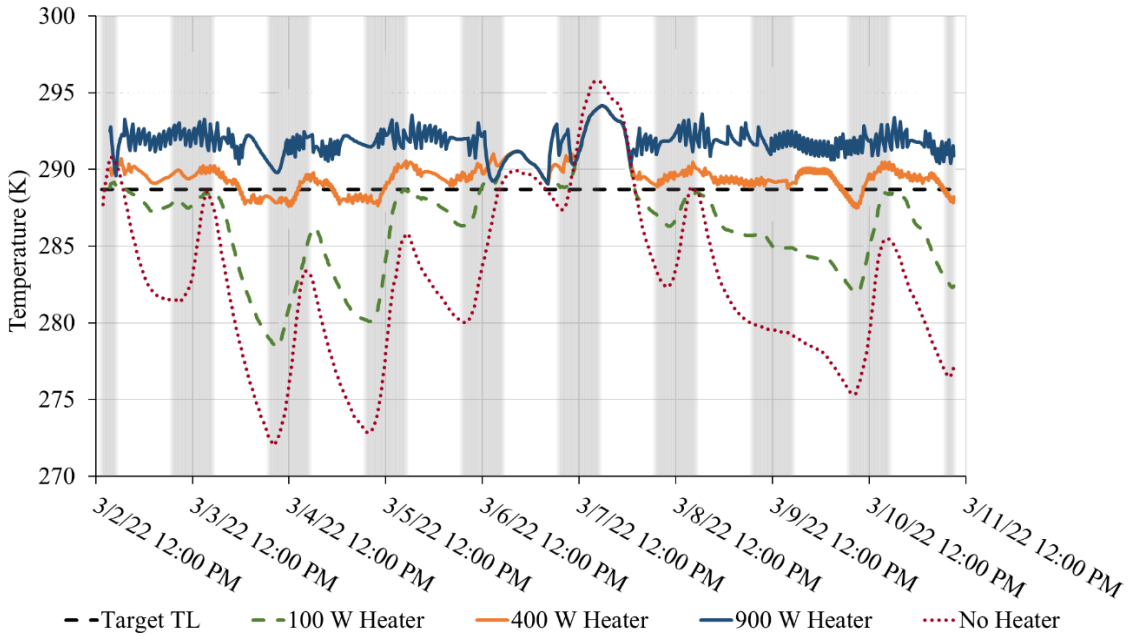

Note. Shaded regions represent occupied hours of Building A (7 AM – 5 PM)

Figure 4.6

Case Study A2 Results (9-Period Moving Average)

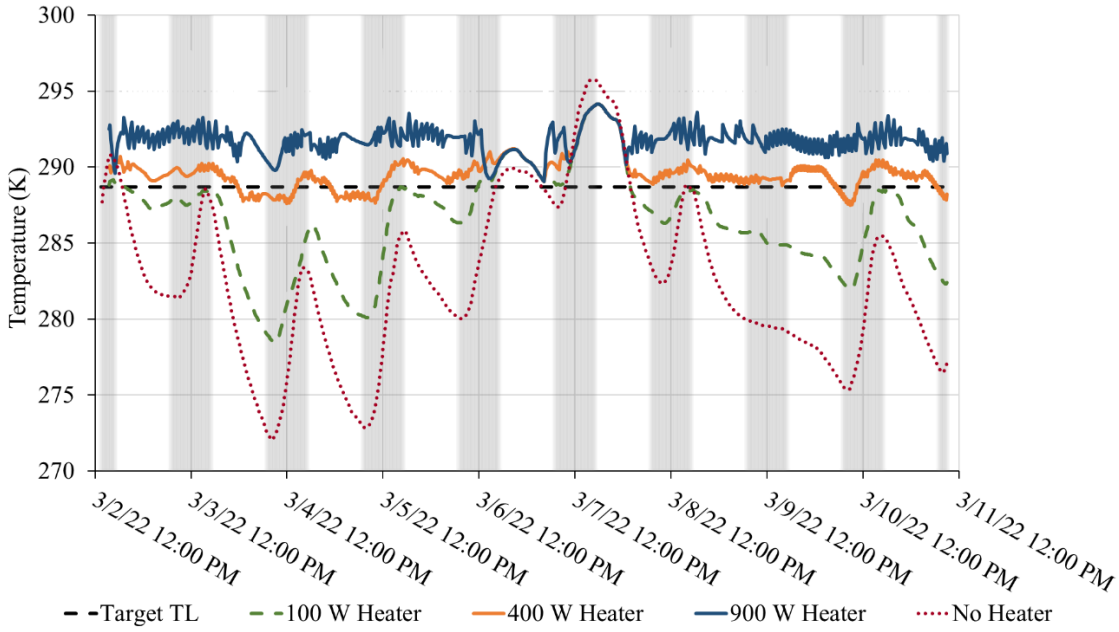

Graphically, the data suggests that the 100 W heater is inadequate to maintain the desired indoor temperature for this configuration and outdoor conditions, while the 400 W and 900 W heaters are sufficient. Consequently, the 900 W has been selected for further study in Case Study A2, and following case studies to account for more severe weather conditions.

4.3.3 Case Study A3

The subsequent case study focuses on implementing setbacks for a 900 W heater (A3) during unoccupied periods of the lower area of Building A, and compares it to the model described in Section 4.3.2, which uses the same 900 W heater without temperature setbacks (A2). The temperature setbacks applied in this case study adhere to the guidelines established by the United States Army, as summarized in Table 4.6.

Specifically, the heater in this case study is configured to maintain an indoor temperature of 60 °F during occupied hours (7 AM – 5 PM) and a temperature of 45 °F during unoccupied hours of Building A [120]. The findings of this case study are presented in Figure 4.7, while Figure 4.8 is used to mitigate the numerical noise in Figure 4.7.

Table 4.6

United States Army's Temperature Regulation Standards

Area Type	Occupied Temperature (°F)	Unoccupied Temperature (°F)
Office (Heating)	72 ± 2	55 ± 5
Office (Cooling)	74 ± 2	85 ± 5
Warehouse (Heating)	60 ± 5	45 ± 5

Note. These temperature standards adhere to Army Regulation (AR) 420-1 [120]

Figure 4.7

Case Study A3 Results

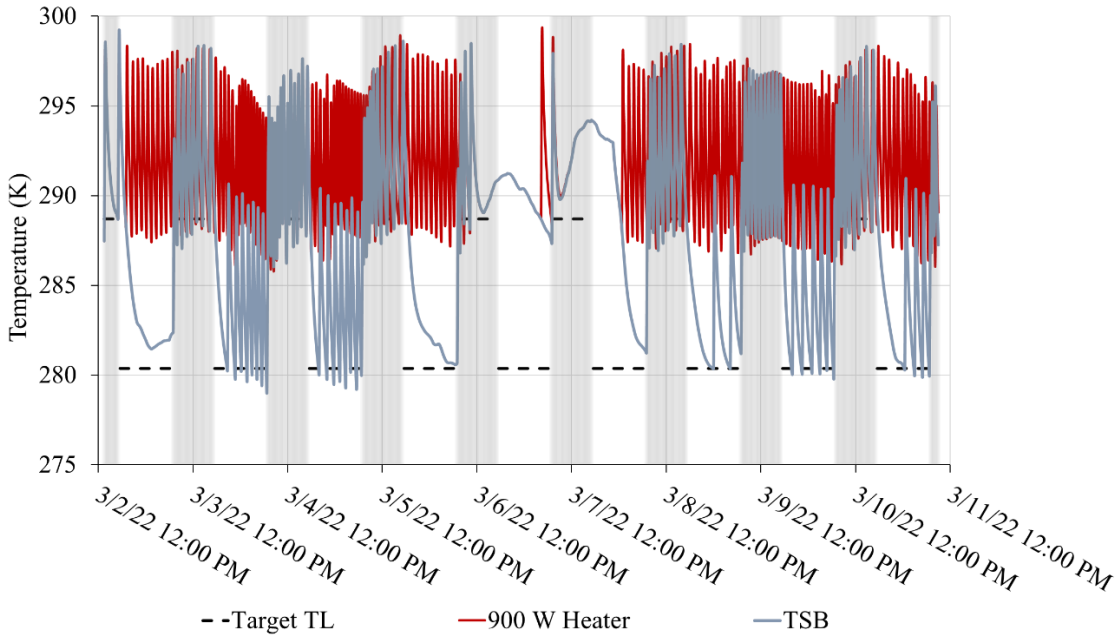

Figure 4.8

Case Study A3 Results (9-Period Moving Average)

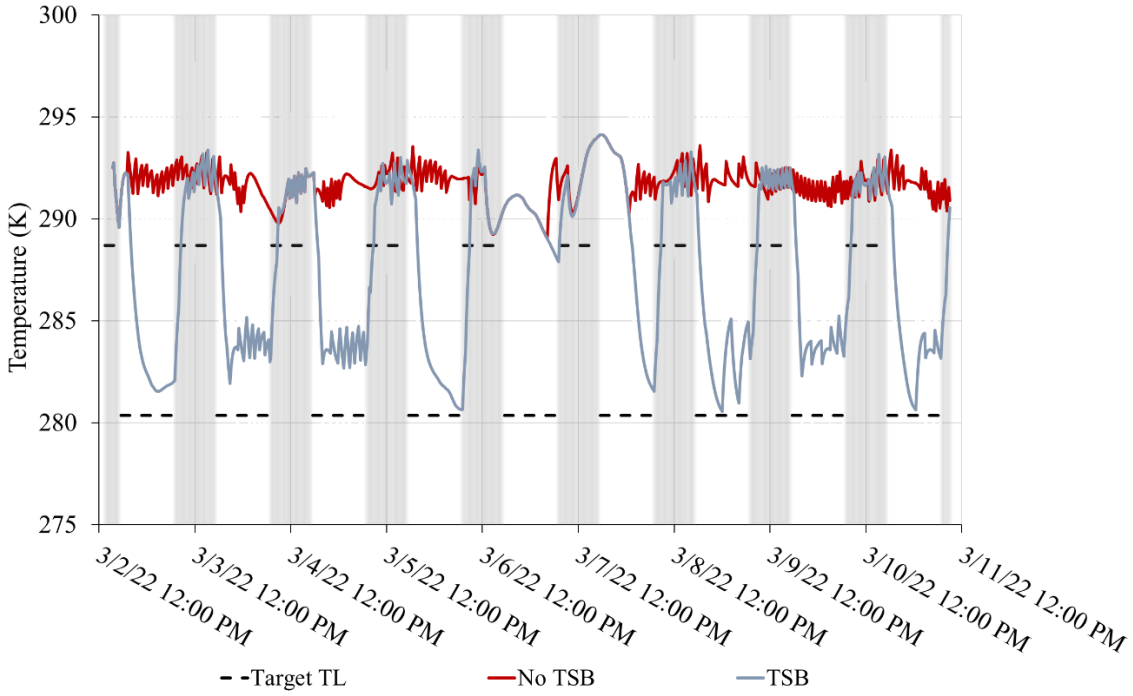

The model forecasts that during the specified data collection period of 10 days between March 2, 2022 and March 11, 2022, the implementation of temperature setbacks (TSB) with the 900 W heater could save 14.85 kWh, which is equivalent to $2.42 based on a rate of 16.25¢ per kWh [121]. Furthermore, the model estimates a reduction of 0.011 metric tons in carbon emissions, considering a rate of $7.09*10^{-4}$ metric tons of CO_2 per kWh rate [122]. Table 4.7 presents the advantages of incorporating temperature setbacks in Building A, as demonstrated by the predicted 44% reduction in energy consumption, cost, and carbon emissions. This table also includes these metrics for the 100 W and 400 W heater analyzed in Case Study A2 to emphasize the effect of this conservation measure.

Table 4.7

Case Study A3 Energy and Financial Analysis Results

Heater Size	Consumed Energy (kWh)		Energy Cost ($)		CO_2 Emissions (metric tons)		Savings
	No TSB	TSB	No TSB	TSB	No TSB	TSB	%
100 W	16.55	9.28	$2.69	$1.51	0.012	0.007	**44%**
400 W	28.3	15.9	$4.60	$2.58	0.020	0.011	**44%**
900 W	36.23	21.38	$5.89	$3.47	0.026	0.015	**41%**

4.3.4 Case Study A4

The objective of the final case study is to determine the optimal heating or cooling periods for the HVAC system, specifically the virtual heater, in Building A. This case study follows the assumptions outlined in Section 4.3.3. Initiating the heating or cooling system at the beginning of the day can lead to suboptimal indoor temperatures during occupied hours, while keeping it on until the end of the day is unnecessary. This is attributed to the thermal capacitance of the building, which induces thermal lag and delayed temperature changes. The findings of this case study are presented in Figure 4.9, with Figures 4.10 and 4.11 providing a closer look at two 24-hour periods within Figure 4.9. Specifically, Figure 4.10 offers a more detailed examination of the time period on March 3, 2022, while Figure 4.11 provides a closer examination of the hours on March 9, 2022.

Figure 4.9

Case Study A4 Results

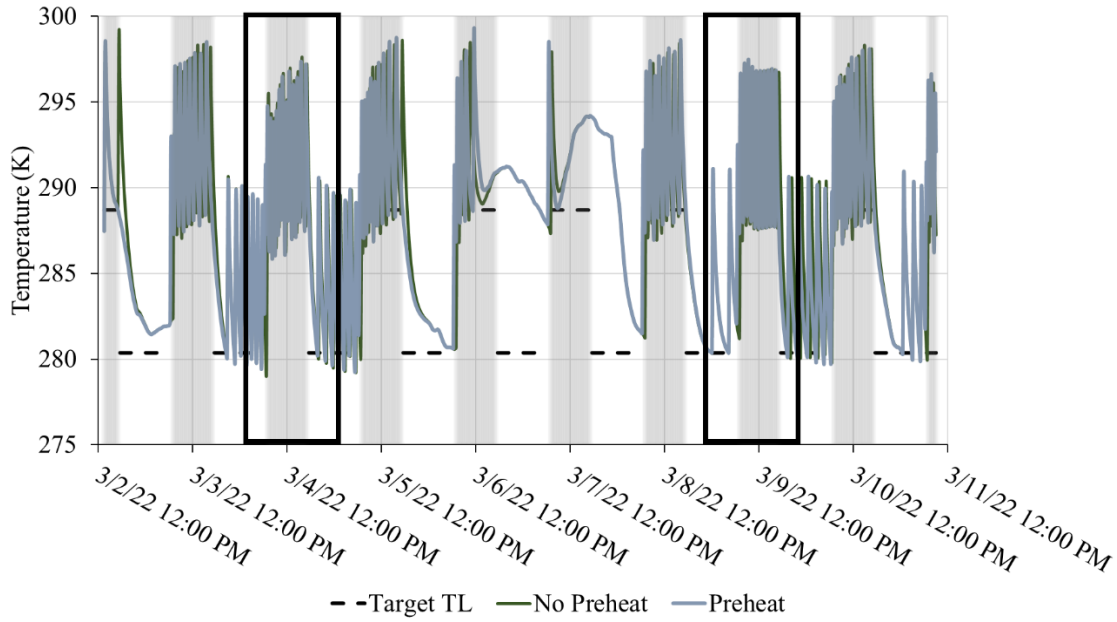

Note. March 3, 2022 (left) and March 9, 2022 (right) are outlined in black and presented in Figures 4.10 and 4.11, respectively.

Evidently, by setting the 900 W heater in Building A to activate at 6:15 AM, the desired occupied temperature of 60 °F can be achieved by the building's start time of 7:00 AM. Conversely, due to the thermal capacitance of Building A, the heater can be switched off at 4:30 PM and still maintain the desired occupied temperature of 60 °F by the end of day at 5:00 PM.

Figure 4.10

First 24-Hour Period of Case Study A4

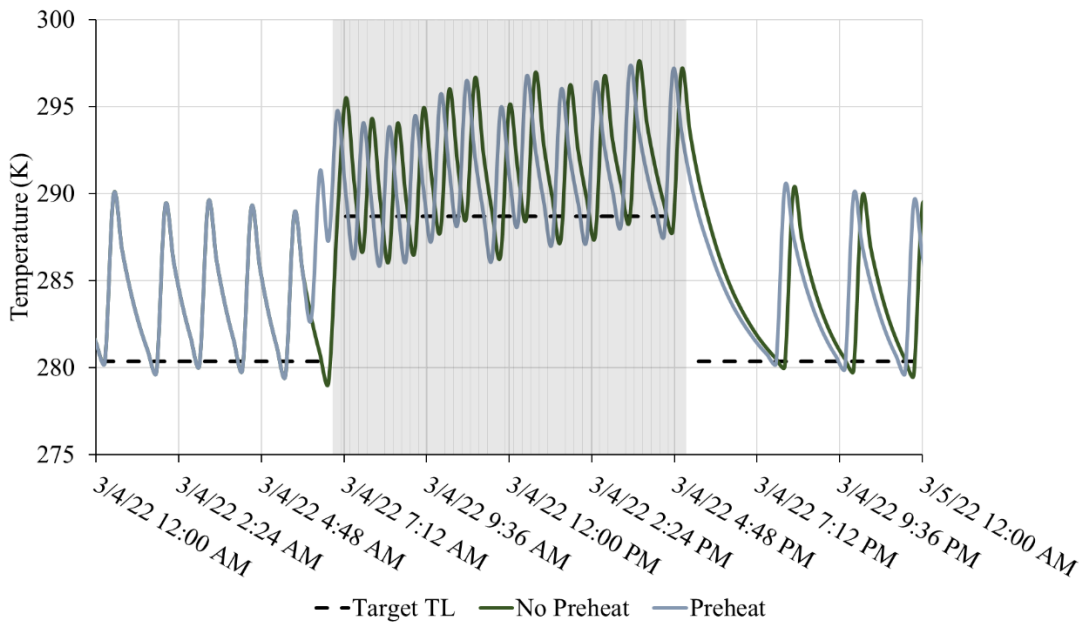

Figure 4.11

Second 24-Hour Period of Case Study A4

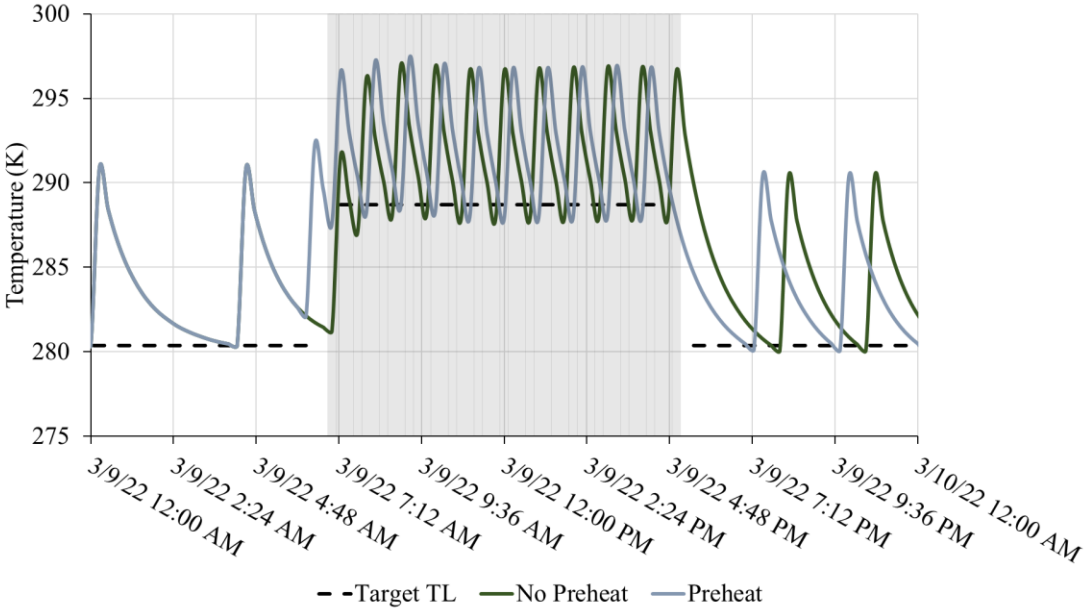

Chapter 5

Data Collection and Energy Modeling Analysis of Building B

5.1 Context of the Chapter

An eQUEST, degree-day, and resistance-capacitance model are developed to demonstrate the feasibility and mechanics of each analytical technique for a building that is more complex than Building A.

5.2 Facility Description of Building B

Building B is a single-story building that was constructed in 1949 under the maintenance of NJDMAVA. The facility consists of eleven rooms, occupying an area of about 8,000 square feet. The building is typically occupied between 7 AM and 5 PM on weekdays (Monday to Friday). The building is heated by a single natural gas-powered boiler located in Room 104, while the building is cooled by an outside electric-powered packaged air-conditioning unit. There is also a wall-mounted mini-split air conditioning unit located in Room 103 to serve as a cooling mechanism to counter the heat generated by the servers in this room. Additional building details are provided in Appendix B.

5.3 eQUEST Model of Building B

A Design Development (DD) Wizard was developed in eQUEST to simulate the monthly electric and natural gas consumption of Building B from January 2019 to December 2022. The simulated results were compared to the observed utility data provided by UtilityAnalytics.

Table 5.1

User Requirements for eQUEST Model

Component	Required Information
Project/Site/Utility	Building location, analysis year, duration of heating/cooling seasons, observed holidays
Building Shell	Building area, number of floors (above/below grade), daylighting controls, orientation, floor-to-floor height, floor-to-ceiling height, roof pitch, overhang projection, zone configuration, roof surface construction, above grade wall construction, ground floor construction, infiltration (shell tightness), top floor ceiling construction, ceiling construction, vertical wall construction, quantity and configuration of exterior doors and dimensions/construction, quantity and configuration of exterior windows and dimensions/construction, exterior window overhangs and fins, window blinds/drapes, roof skylights, heating/cooling season schedules and magnitude, types of room areas and design maximum occupancy and design ventilation, interior and exterior end uses, interior lighting, office equipment, miscellaneous equipment, computer server, exterior lighting loads and profiles, and domestic water heating hourly profiles
Air-Side System(s)	Unoccupied/occupied indoor temperature setpoints during heating/cooling seasons, thermostat location, indoor and supply cooling/heating design temperatures, minimum design flow, overall size, typical unit size, condenser types, efficiency of cooling equipment, size, typical unit size, efficiency of heating equipment, supply fan power, MTR efficiency, fan flow, OSA, HVAC system(s) schedules, economizer(s) and humidity control
HW Plant Equipment	HW loops head, design DT, pump configuration, HW loop flow, number of system pumps, motor efficiency, boiler type and fuel source, boiler efficiency, boiler output, HW system control and schedule
DHW Equipment	Heater specifications (heater fuel, heater type, hot water use, input rating, efficiency specifications, thermal efficiency), storage tank capacity, standby loss, insulation R-value, supply and inlet water temperatures, percentage of recirculation pumping

Figures 5.1 and 5.2 present a 48-month comparison of simulated and observed electric and natural gas consumption from January 2019 and December 2022. The electric consumption simulation exhibited an average monthly error of 37.2%, while the natural gas consumption simulation displayed an average monthly deviation of 63.2%.

Figure 5.1

Simulated and Observed Electric Consumption over Time

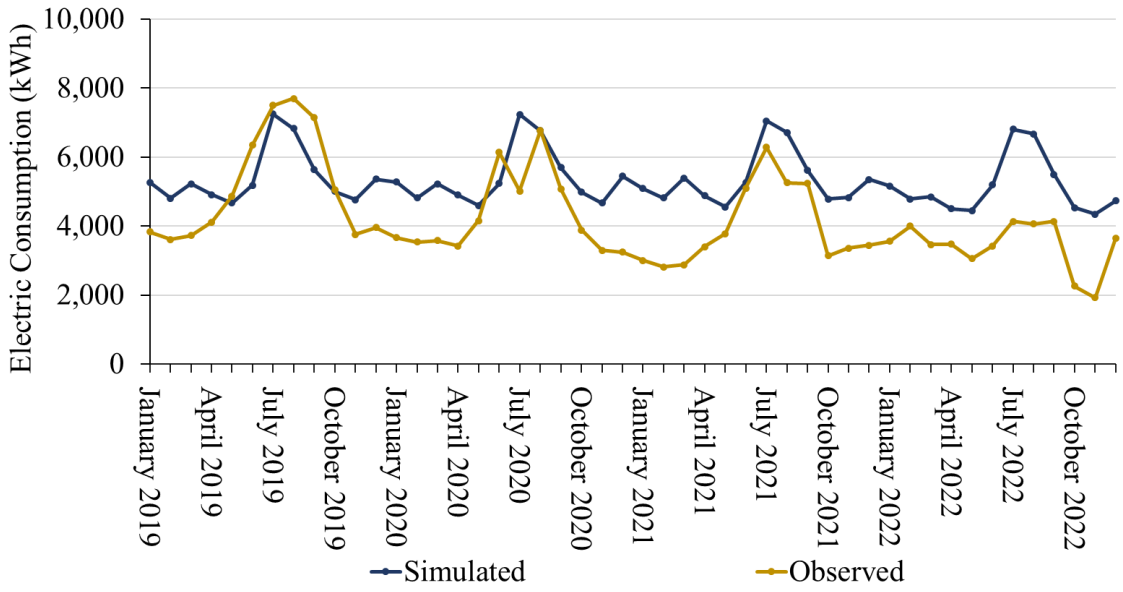

Figure 5.2

Simulated and Observed Natural Gas Consumption over Time

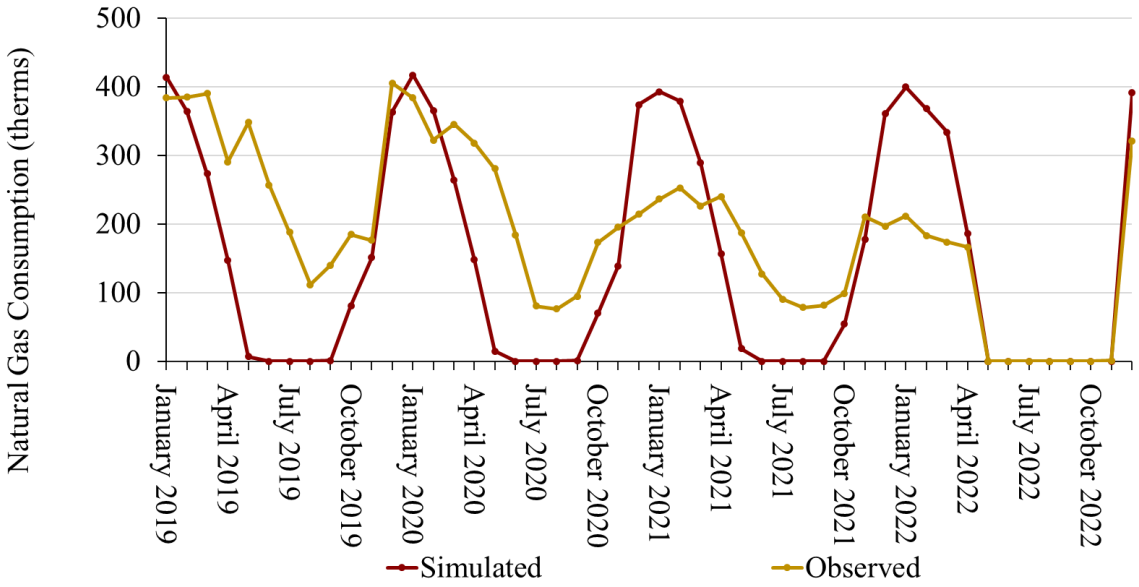

The model's forecast, illustrated in Figure 5.3, suggests that from January 2019 to December 2022, introducing temperatures setbacks (TSB) regulated by the United States Army (see Table 5.2) during the unoccupied hours at Building B could lead to a significant reduction in its electric consumption by 13,190 kWh, resulting in potential cost savings $1,978, considering the facility's average utility charge rate of 15¢ per kWh. Additionally, the implementation of TSB is estimated to reduce carbon emissions by 9.35 metric tons of CO_2 per kWh during the same period, based on a rate of 7.09×10^{-4} metric tons of CO_2 per kWh [122]. However, the model's prediction, illustrated in Figure 5.4, suggests that from this same time period, implementing temperature setbacks during the unoccupied hours at Building B could yield an increase in natural gas consumption, amounting to 513 therms. This translates to potential increase in cost of $231, considering the facility's average utility charge rate of 45¢ per kWh. Furthermore, the

implementation of temperature setbacks is estimated to result in an increase of 2.7 metric tons of CO_2 emissions during the same period, based on a rate of 5.30×10^{-3} metric tons of CO_2 per therms of natural gas [122]. These findings are summarized in Table 5.3.

Figure 5.3

Results of Electric Consumption Reduction from Temperature Setbacks

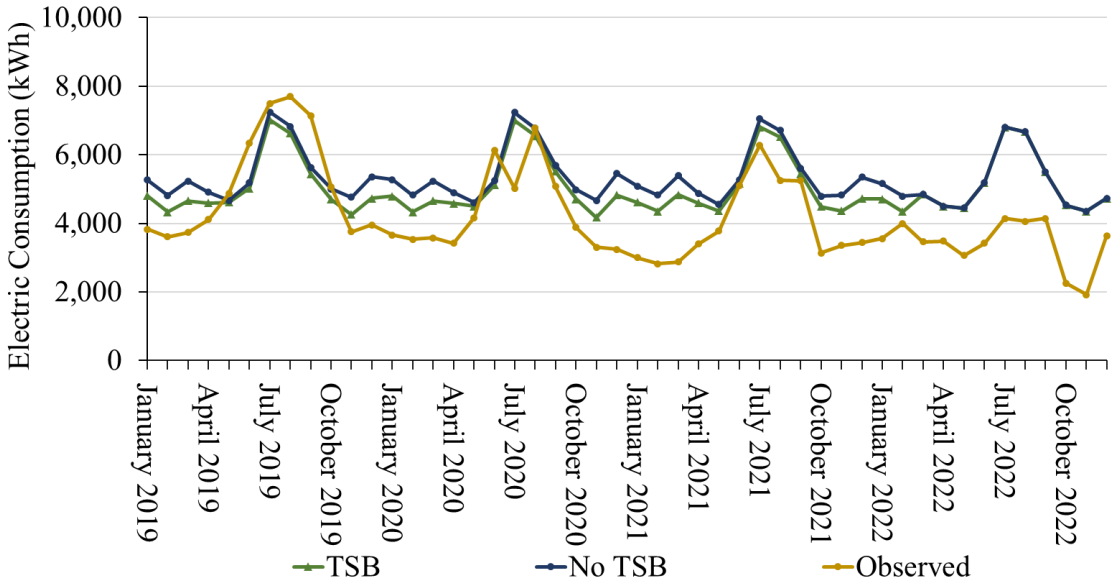

Table 5.2

Occupied and Unoccupied Temperature Setpoints at Building B

Heating		Cooling	
Occupied (°F)	Unoccupied (°F)	Occupied (°F)	Unoccupied (°F)
72	55	80	85

Note. The occupied cooling setpoint does not adhere to Army Regulation (AR) 420-1 [120].

Figure 5.4

Results of Natural Gas Consumption Increase from Temperature Setbacks

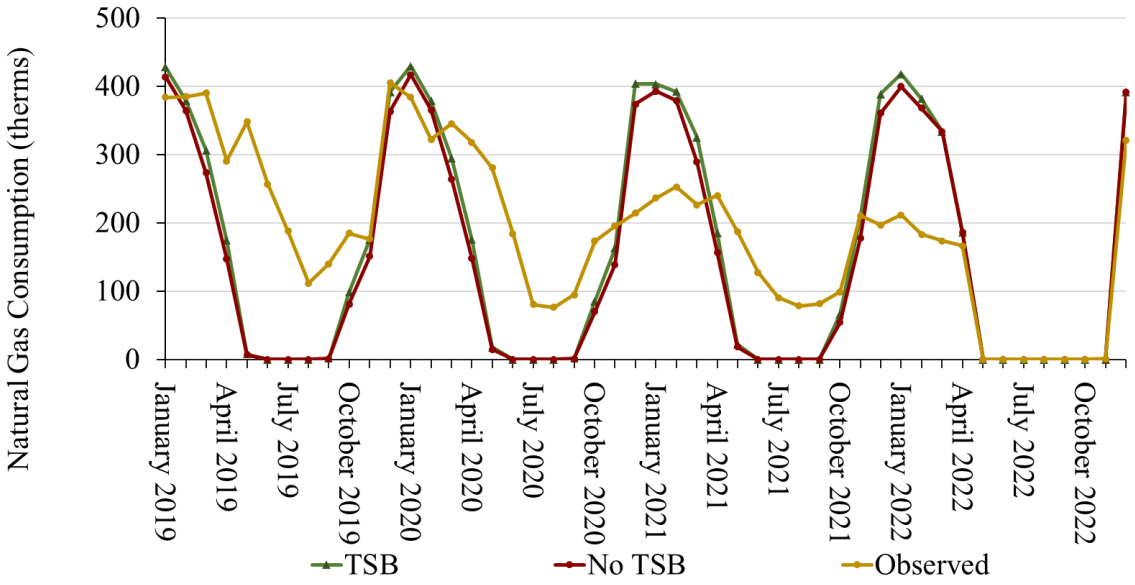

Table 5.3

Energy and Financial Analysis Results of eQUEST Case Study

Fuel Source	Consumed Energy (kWh)		Energy Cost ($)		CO_2 Emissions (metric tons)		Savings
	No TSB	TSB	No TSB	TSB	No TSB	TSB	%
Electric (kWh)	255,650	242,460	$38,348	$39,400	181.3	171.9	**5%**
Nat. Gas (therms)	7,105	7,618	$3,197	$3,428	37.7	40.4	**-7%**

5.4 Degree-Day Model of Building B

A degree-day model of Building B was constructed using obtained utility data such as electric and natural gas consumption, along with historical weather information such as heating (HDDs) and cooling degree days (CDDs) over the 54 months spanning from January 2019 to June 2023. Historical utility data was provided by UtilityAnalytics. Daily HDDs and CDDs were generated by BizEE's degree-day generation tool, using a

65 °F base temperature and were aligned with the corresponding utility billing periods. Since the building is primarily cooled by an electricity powered packaged VAV air conditioning unit and heated by a natural gas powered condensing boiler, HDDs are plotted against natural gas consumption and CDDs are plotted against electric consumption to identify a relationship between these values. Contrarily, HDDs are plotted against electric consumption and CDDs are plotted against natural gas consumption to identify their respective baseline consumptions, which represents the minimum amount of energy that the building consumes for essential operations, including heating, cooling, and lighting. Data points with low HDDs or CDDs may make this level of analysis difficult, so Figure 5.5 displays HDDs against CDDs to identify the "zero point," which may skew the data. HDDs and CDDs were plotted against natural gas and electric consumption, specifically: 1) HDDs vs. natural gas consumption, 2) CDDs vs. electric consumption, 3) CDDs vs. natural gas consumption, and 4) HDDs vs. electric consumption. These plots are discussed in more detail in the following subsections.

Figure 5.5

Cooling Degree-Days vs. Heating Degree-Days

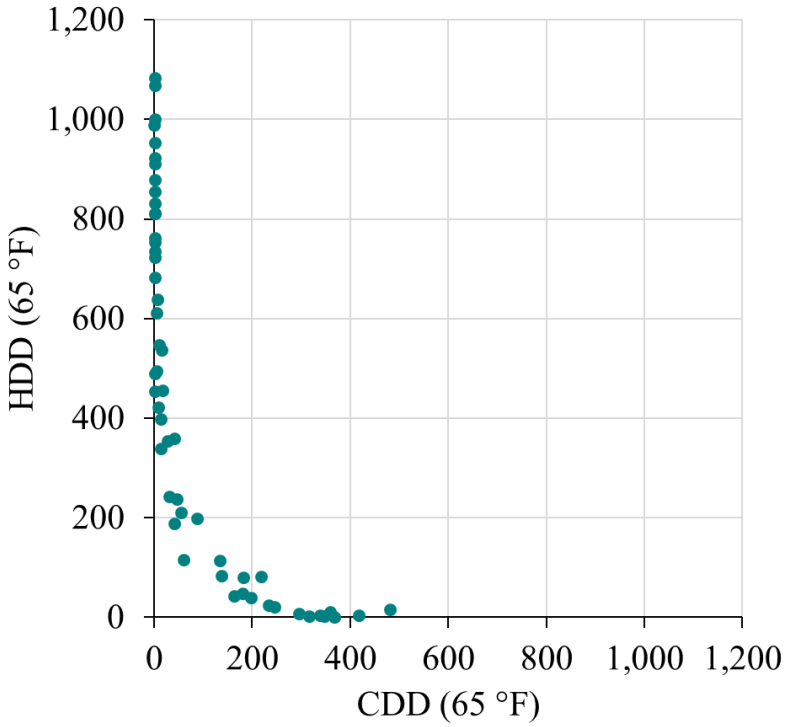

5.4.1 Heating Degree-Days vs. Natural Gas Consumption

The natural gas consumption of Building B during the specified period of 54 months, from January 2019 and June 2023, was plotted against heating degree-days (HDDs). However, the data between May 2022 and November 2022 were excluded from the data set since the condensing boiler at Building B was turned off at that time. The original data set exhibited a weaker correlation ($R^2 = 0.48$), as depicted in Figure 5.6, suggesting a possible change in building operations during that period.

Figure 5.6

Heating Degree-Days vs. Natural Gas Consumption for Building B

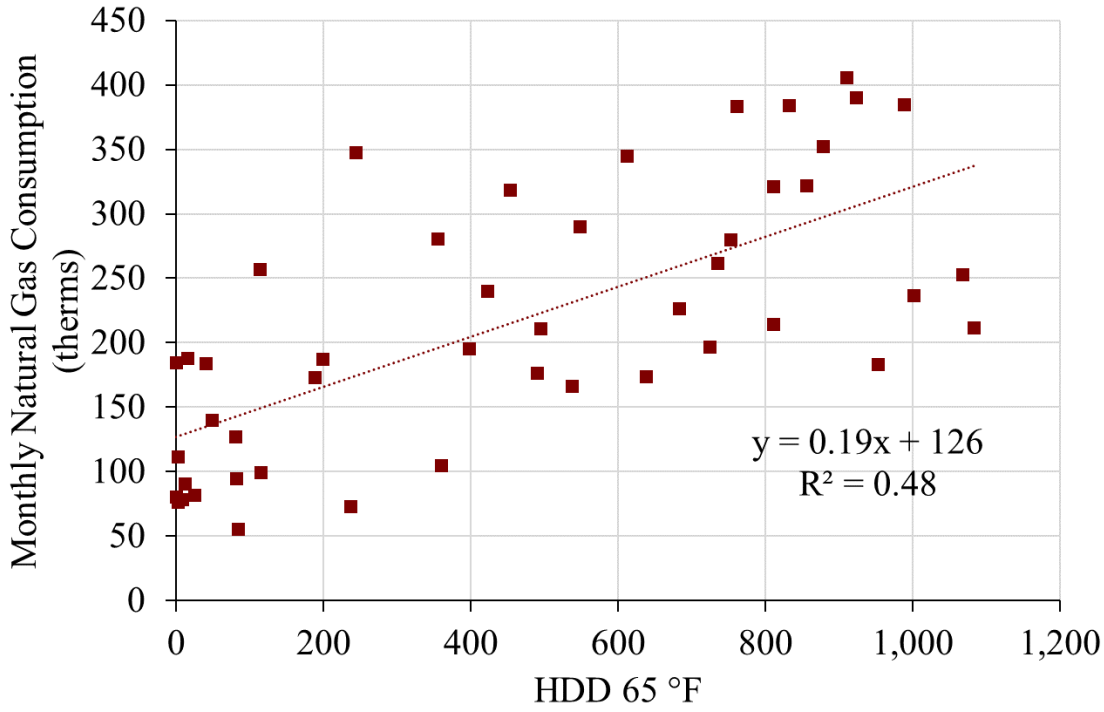

The change in building operation was identified in July 2020, potentially influenced by the response of the building operator of Building B to the COVID-19 pandemic, which was declared a national emergency in the United States in March 2020. Consequently, the original data set was divided into two sets, as illustrated in Figure 5.7. The first set of data (Pre-COVID-19) encompasses data points from January 2019 to June 2020, represented by gold circles. The second set of data (Post-COVID-19) consists of data points from July 2020 to June 2023, depicted by red circles, excluding data points between May 2022 and November 2022. The coefficient of determination (R^2) for the first and second data sets is 0.73 and 0.66, respectively, which supports the occurrence of a shift in building operations at Building B.

Figure 5.7

Heating Degree-Days vs. Natural Gas Consumption for Building B (Split Data)

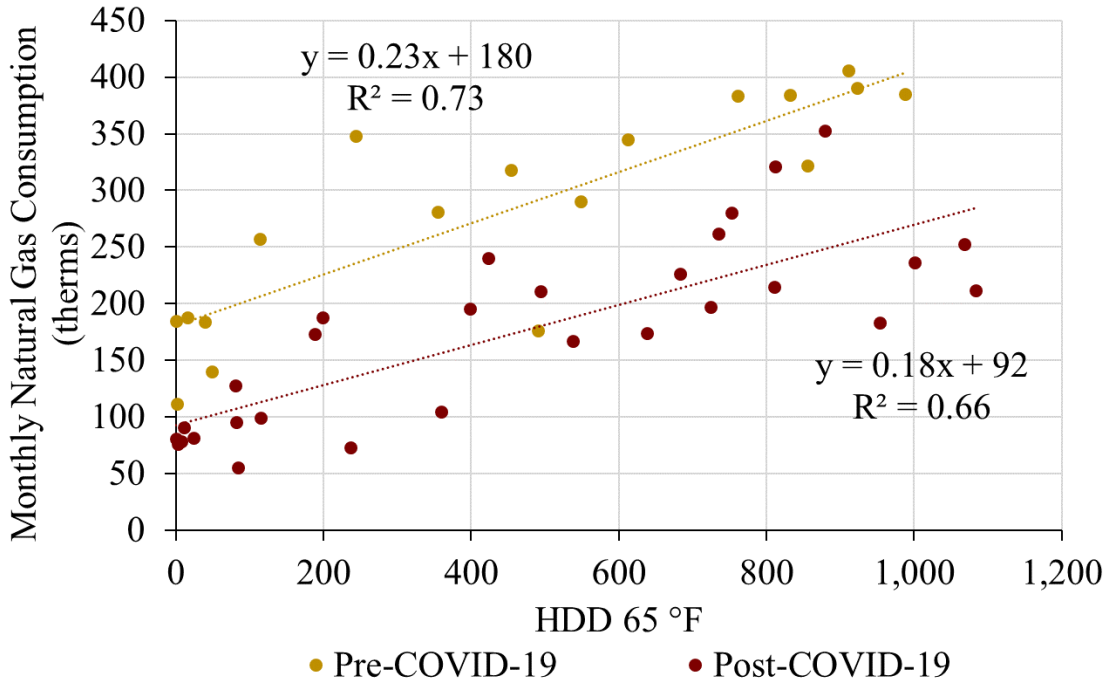

5.4.2 Cooling Degree-Days vs. Electric Consumption

The electric consumption of Building B during a specified period of 54 months, from January 2019 and June 2023, was plotted against cooling degree-days (CDDs). The original data set exhibited a weaker correlation ($R^2 = 0.55$), as depicted in Figure 5.8, indicating a potential change in building operations during that period.

Figure 5.8

Cooling Degree-Days vs. Electric Consumption for Building B

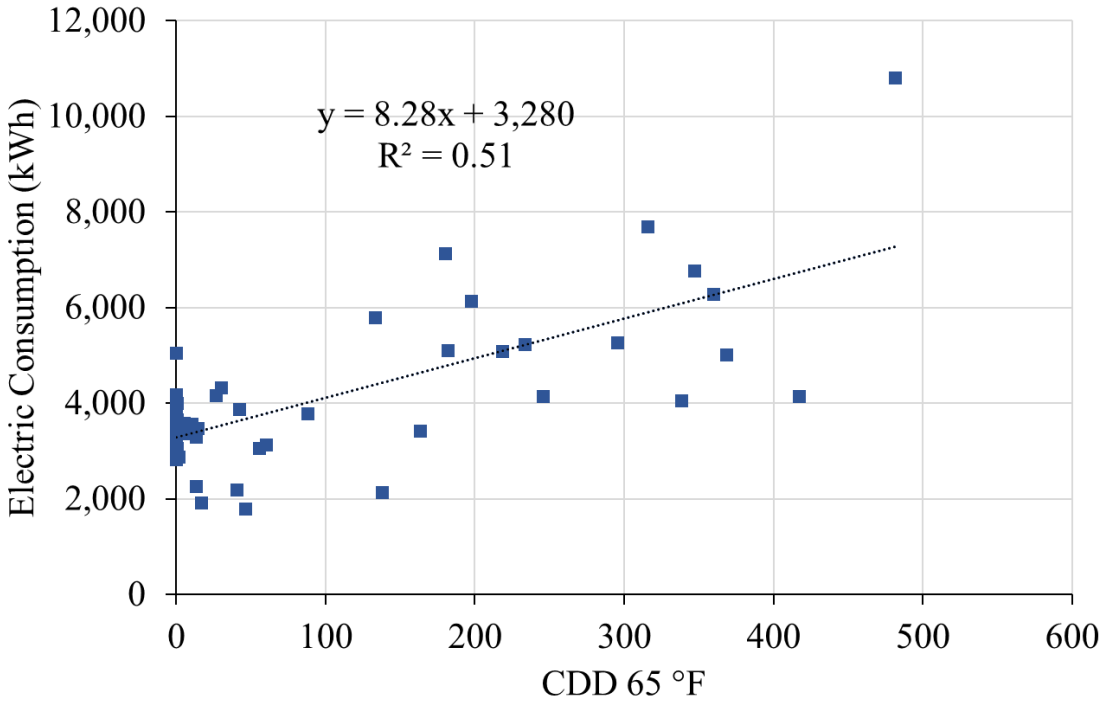

The previously identified change in building operation occurred in July 2020 and temperature setbacks were enacted in March 2022. Consequently, the initial data set was divided into three sets, as depicted in Figure 5.9. The first set of data (Pre-COVID-19), second set (Post-COVID-19), and third set (Temp. Stbcks.) have slopes of 14.52, 7.69, and 2.70 with R^2 values of 0.94, 0.85, and 0.13, respectively. These changes indicate changes in building operations at Building B in July 2020 and March 2022. However, R^2 is not a robust measure to validate the change in building operations since the slope of this trendline is nearly zero.

Figure 5.9

Cooling Degree-Days vs. Electric Consumption for Building B (Filtered Data)

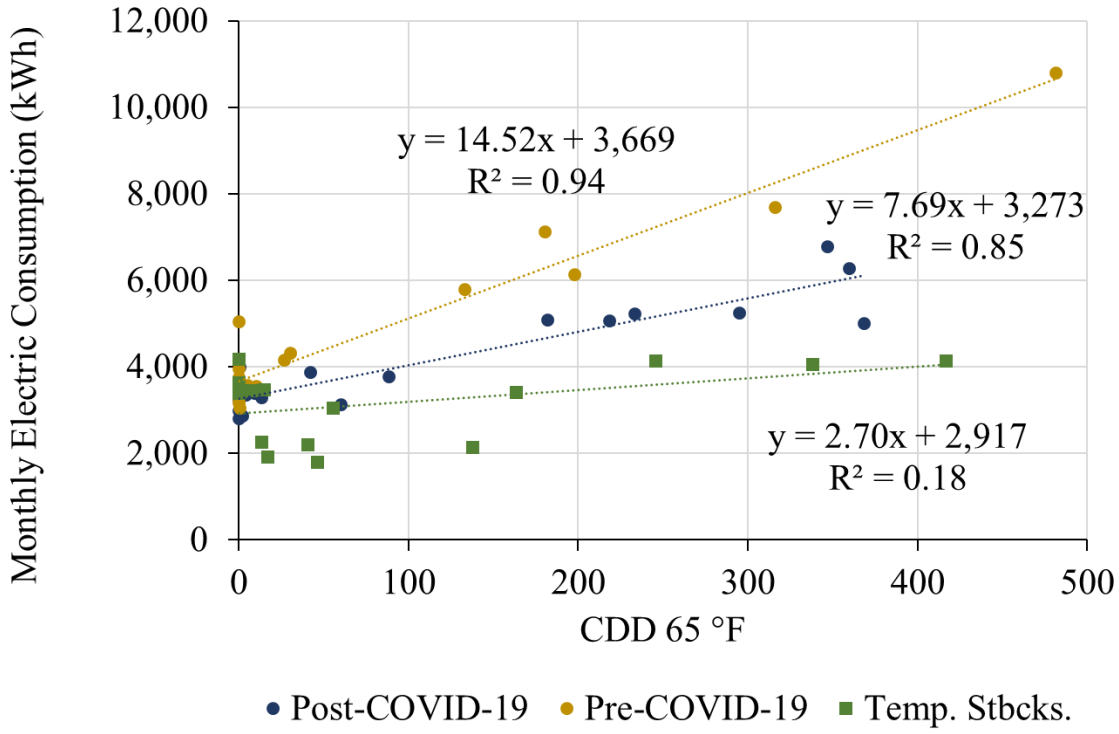

5.4.3 Cooling Degree-Days vs. Natural Gas Consumption

The natural gas consumption of Building B during a specified period of 54 months, from January 2019 and June 2023, was plotted against CDDs. However, the data points between May 2022 and November 2022 were excluded from the analysis. Moreover, data points with less than 25 CDDs were not included in the fitting of the regression line, as depicted in Figure 5.10. Figure 5.5 illustrates that a threshold of 25 CDDs for the fitted data points was deemed appropriate (slope is approaching zero). Based on the intercept of the fitted line, the monthly baseline natural gas consumption was determined to be about 133 therms.

Figure 5.10

Cooling Degree-Days vs. Natural Gas Consumption for Building B

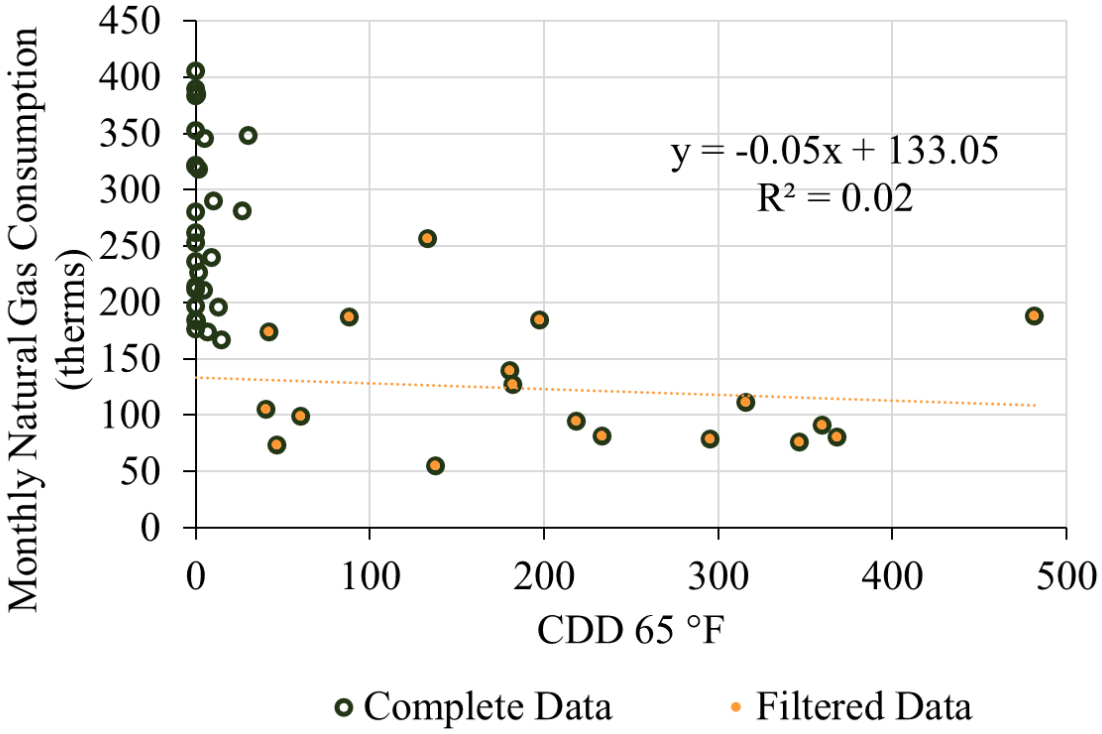

5.4.4 Heating Degree-Days vs. Electric Consumption

The electric consumption of Building B during a specified period of 54 months, from January 2019 to June 2023, was plotted against HDDs. However, data points with less than 50 CDDs were not considered when fitting through these data, as depicted in Figure 5.11. Figure 5.5 illustrates that a threshold of 50 HDDs for the data points was deemed appropriate (slope is approaching infinity). Based on the intercept of the fitted line, the monthly baseline electric consumption was determined to be about 3,654 kWh.

Figure 5.11

Heating Degree-Days vs. Electric Consumption for Building B

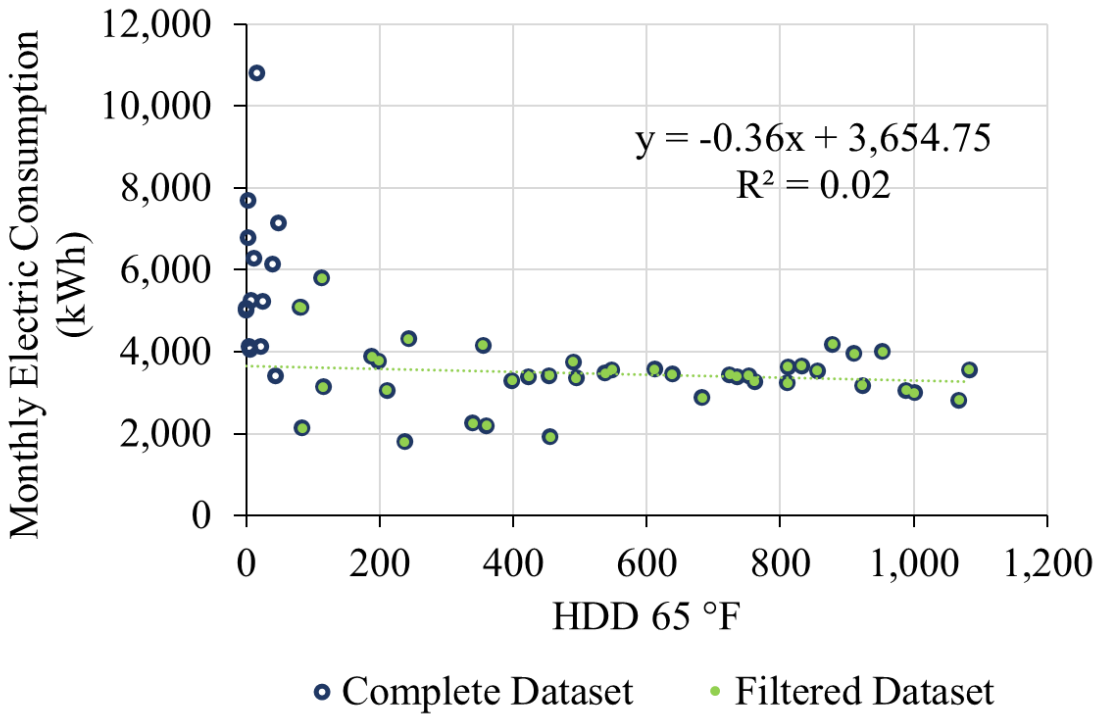

5.5 Resistance-Capacitance Model of Building B

Figure 5.12 shows that thirteen HOBO UA2300 indoor temperature sensors (A through N) were deployed within Building B, while a HOBO MX2304 outdoor temperature sensor, solar radiation shield, and a Wyze Cam v3 security camera were attached to tripods (A0 and B0) that were set up outside, as shown in Figure 5.13. These tripods were situated on the northeast and southwest sides of Building B where the respective electricity and natural gas meters are located. All interior and exterior doors were closed following the equipment's deployment. Data collection began on February 16, 2022, at 12:00 PM, and continued until March 2, 2022, at 9:15 AM. Following a modification to the building's heating

setpoints, data collection was resumed on March 16, 2022, at 12:00 PM, and concluded on April 6, 2022, at 9:00 AM.

Figure 5.12

Location of Indoor and Outdoor Temperature Sensors at Building B

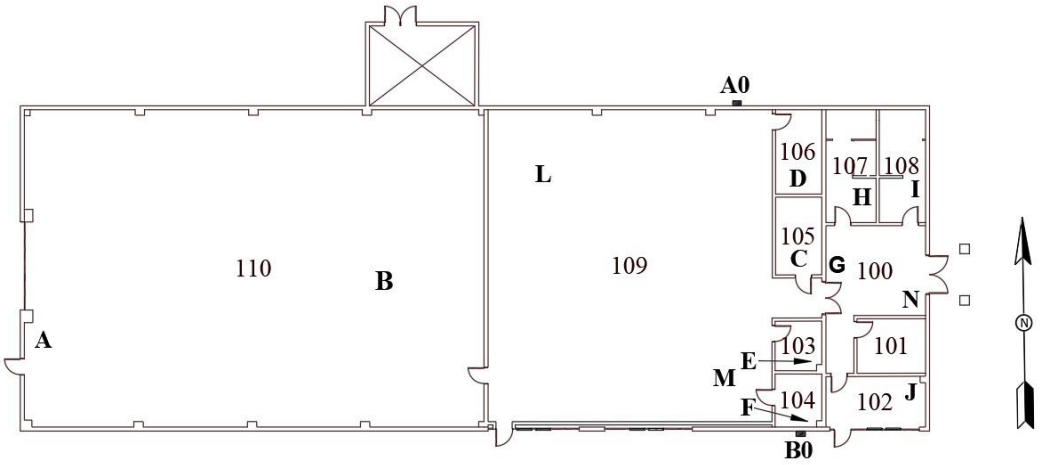

Figure 5.13

Equipment Setup of A0 (left) and B0 (right) tripods at Building B

The average zonal temperature data displayed in Figure 5.14 suggest that Building B can be represented by five capacitive elements (zones) that interconnected with each other, the outside, and the ground via four distinct resistive elements. This configuration creates a four resistor five capacitor model (4R5C). The subsequent plots demonstrate that the average temperatures of the zones reflect the temperature across large volumes within those zones. A schematic of the model is shown in Figure 5.15. The capacitive elements are indicated in blue. The resistive elements are represented by red single arrows indicating the direction of positive heat flow. The heat transfer mechanisms involved include conduction, convection, air infiltration, ventilation, and solar radiation through the building's ceiling, roof, floor, and walls. However, it is important to note that solar radiation was not specifically addressed in this study. The determination of each capacitive zone and the additional assumptions applied in the 4R5C model elaborated in the subsequent subsections.

Figure 5.14

Average Zonal Indoor Temperature Data at Building B

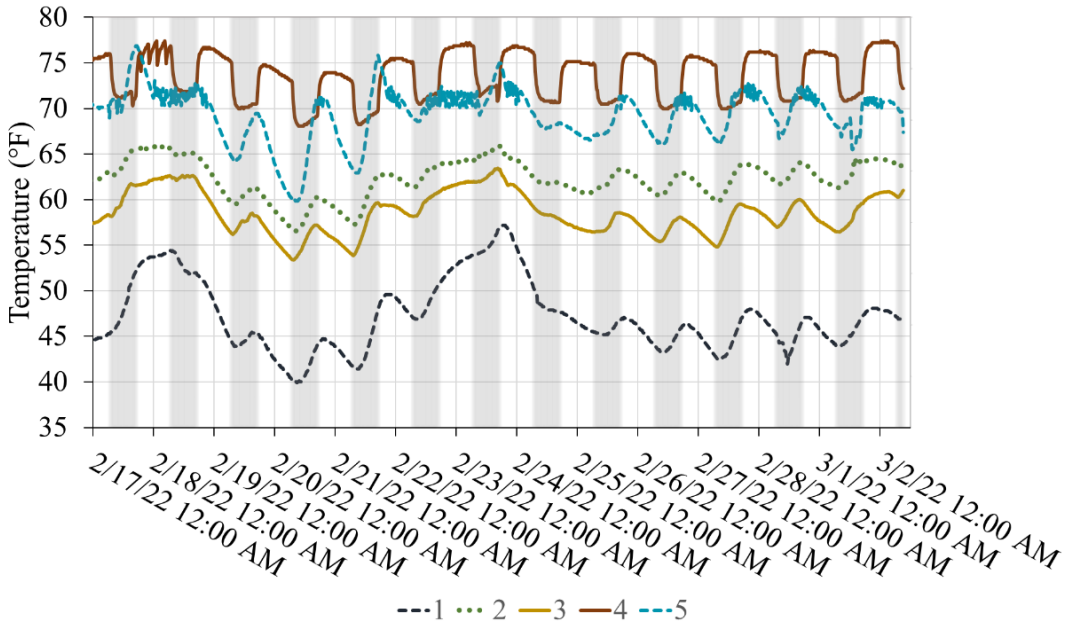

Figure 5.15

Heat-Balance Model of Building B

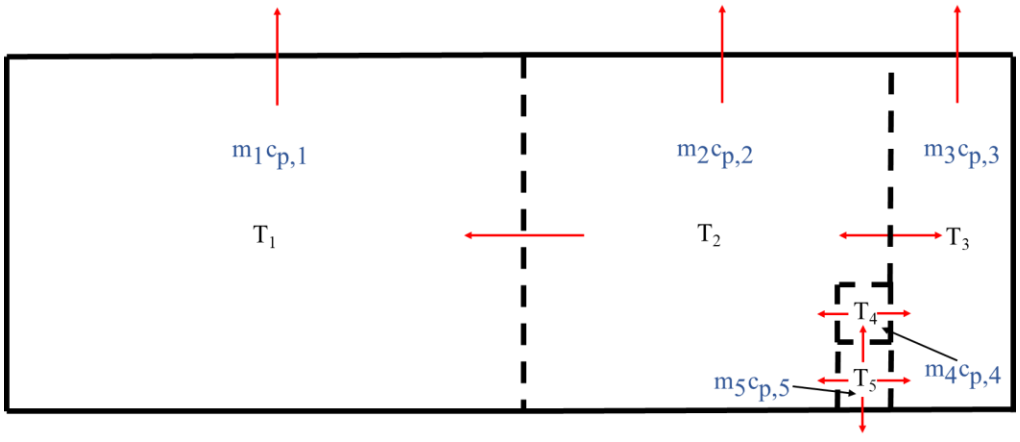

Figure 5.16 displays the indoor temperature data for Zone 1, which corresponds to unconditioned storage area (Room 110) in Building B. In this zone, two HOBO UA2300

indoor temperature sensors, labeled as A and B, were deployed for data collection. Despite minor fluctuations, a clear correlation can be observed among the recorded temperatures in this particular zone.

Figure 5.16

Indoor Temperature Data for Zone 1

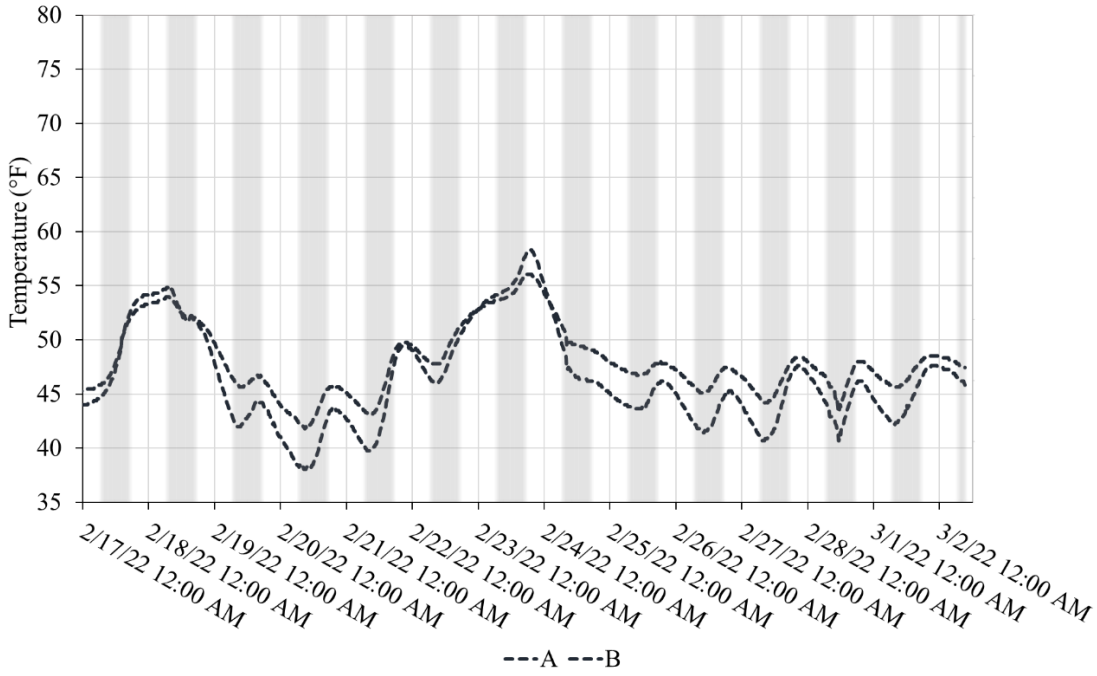

Figure 5.17 displays the indoor temperature data for Zone 2, which consists of a conference room (Room 104), a sprinkler valve room (Room 106), and a storage room (Room 105). In this zone, five HOBO UA2300 indoor temperature sensors, labeled as C, D, K, L, M, and O, were deployed for data collection. Despite minor temperature fluctuations, a clear correlation can be observed among the recorded temperatures in this particular zone.

Figure 5.17

Indoor Temperature Data for Zone 2

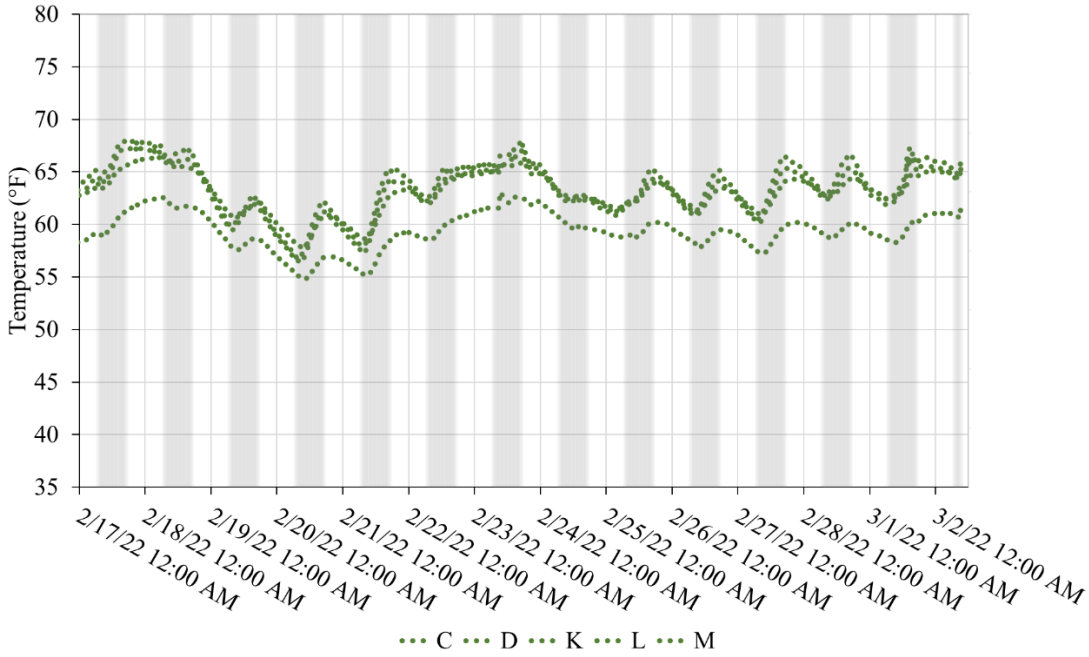

Figure 5.18 displays the indoor temperature data for Zone 3, which consists of a lobby area (Room 100), two offices (Rooms 101 and 102), and two restrooms (Rooms 108 and 109). In this zone, five HOBO UA2300 indoor temperature sensors, labeled as G, H, I, J, and N, were deployed for data collection. Although there is a notable temperature spike in Room 102 (J) during the building's occupied hours (shaded region in figure), likely caused by solar radiation, there is a distinct correlation observed among the recorded temperatures in this particular zone.

Figure 5.18

Indoor Temperature Data for Zone 3

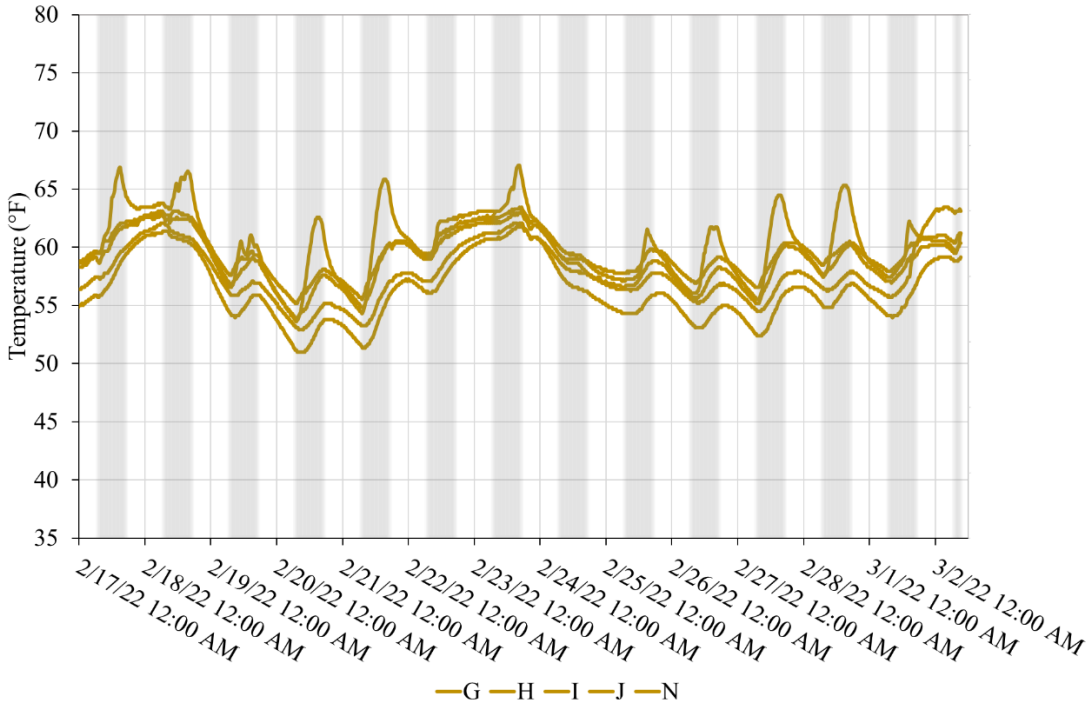

Figure 5.19 displays the indoor temperature data for Zone 4, which corresponds to the server room (Room 103). In this zone, a single HOBO UA2300 indoor temperature sensor, labeled as E, was deployed for data collection. This zone is distinct due to the presence of a split-system heat pump, specifically the LG Inverter V, which is programmed to maintain an indoor temperature of 61 °F during the occupied hours and 70 °F during the unoccupied hours. This unique temperature regulation system is in place to counteract the heat generated by the servers in this zone, thus warranting its classification as a separate zone.

Figure 5.19

Indoor Temperature Data for Zone 4

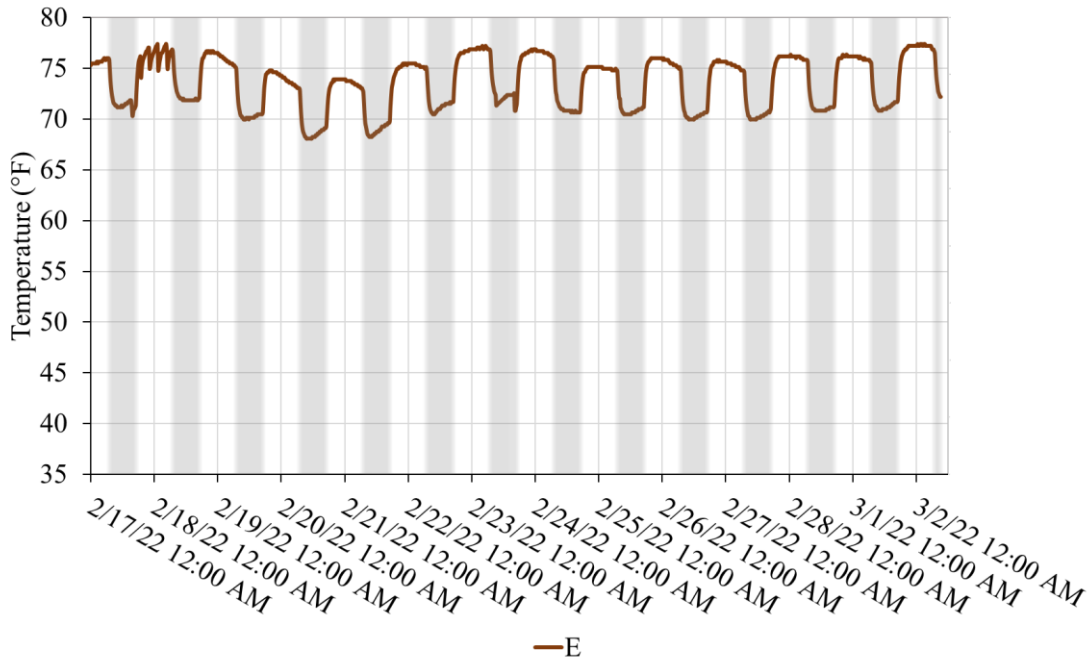

Figure 5.20 displays the indoor temperature data for Zone 5, which corresponds to the boiler room (Room 104). In this zone, a single HOBO UA2300 indoor temperature sensor, labeled as F, was deployed for data collection. This zone is distinct due to the presence of a condensing boiler, specifically the Aerco MLX EXT 321, that is responsible for the heating operations of building. The unit is designed to supply water at a temperature of 130 °F when the outdoor temperature is above 32 °F and 160 °F when it is below 32 °F. This is a distinctive temperature control mechanism that may account for the atypical temperature behavior observed in this zone, thus warranting its classification as a separate zone.

Figure 5.20

Indoor Temperature Data for Zone 5

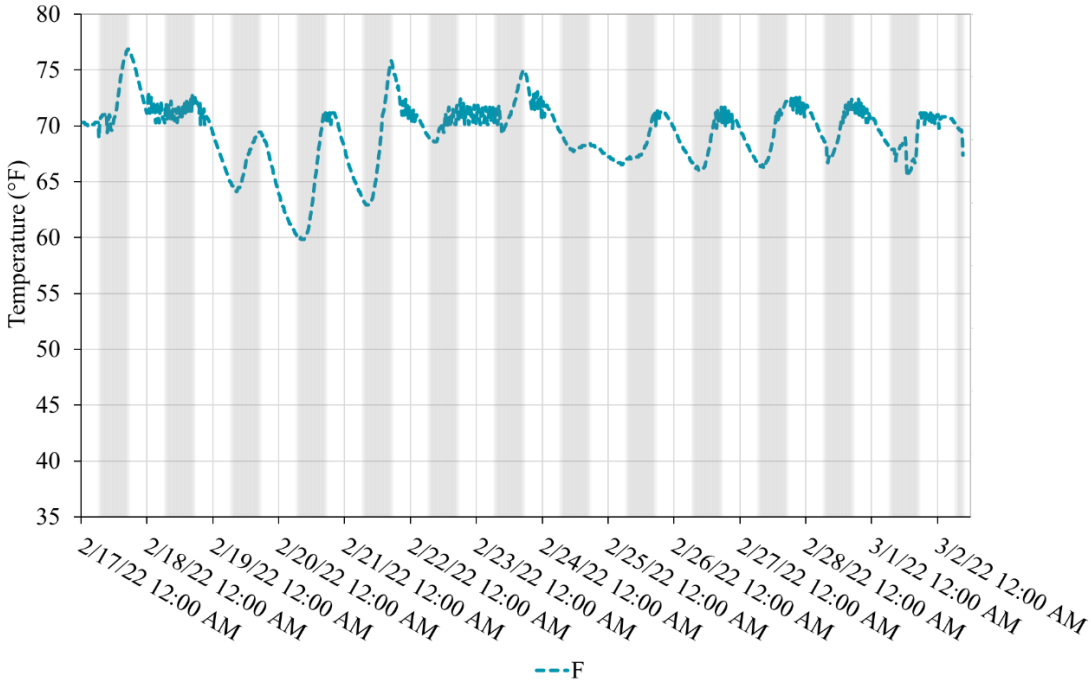

Non-transient heat transfer conditions were assumed in the 4R5C model. The ground temperature, T_G, was considered to be constant at 55 °F, while the outdoor temperature was regarded as a time-dependent variable. The thermal resistances of the ceiling, roof, floor, and exterior walls were designated as R_C, R_R, R_F, and R_{EW}, respectively, and were selected based on the climate zone 4 insulation standards established by the United States Department of Energy [116]. These standards were introduced in Table 4.1. The thermal capacitances of each zone, as well as air infiltration in the building, were fitted using data solver to account for errors in the model. The temperature of the five capacitive zones of Building B are the unknown values that the model solves for, which are presented in Figure 5.21 through 5.25.

Figure 5.21

Modeled Temperature for Zone 1

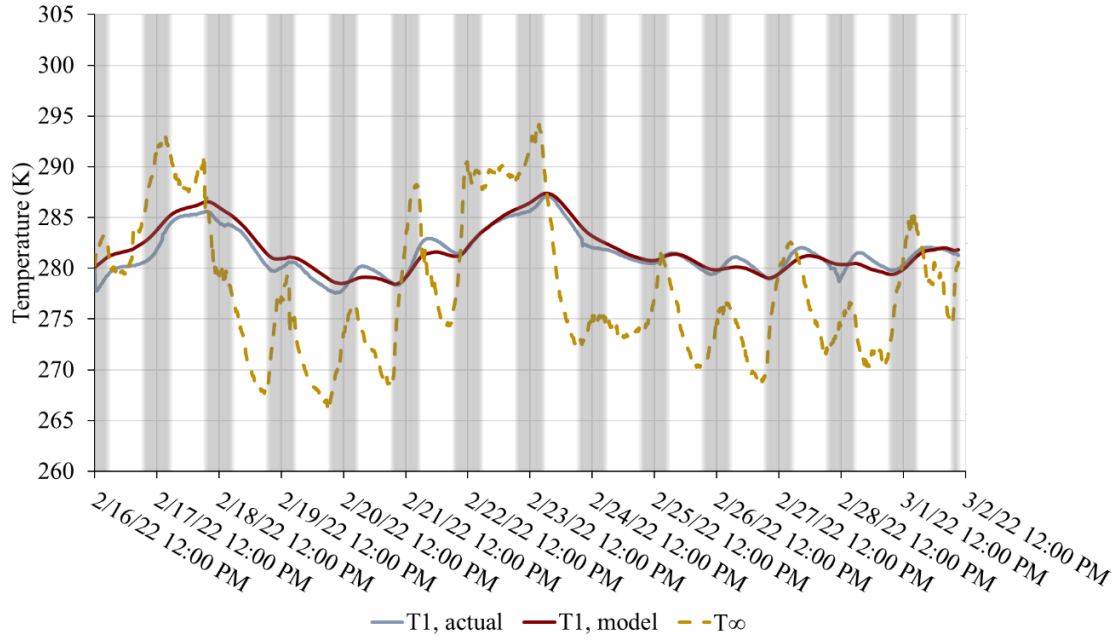

Figure 5.22

Modeled Temperature for Zone 2

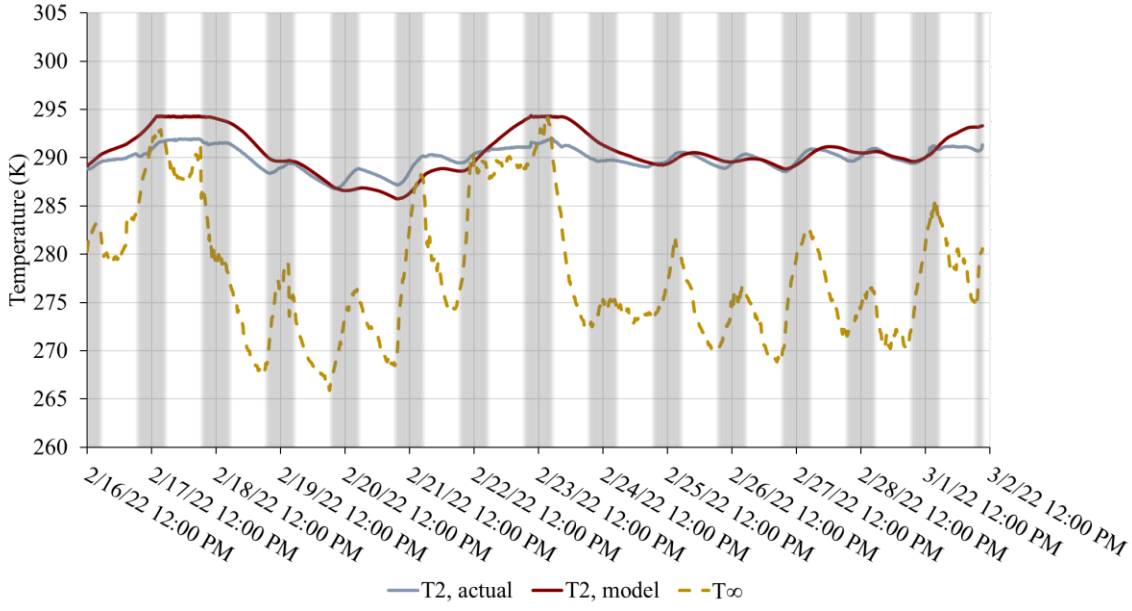

Figure 5.23

Modeled Temperature for Zone 3

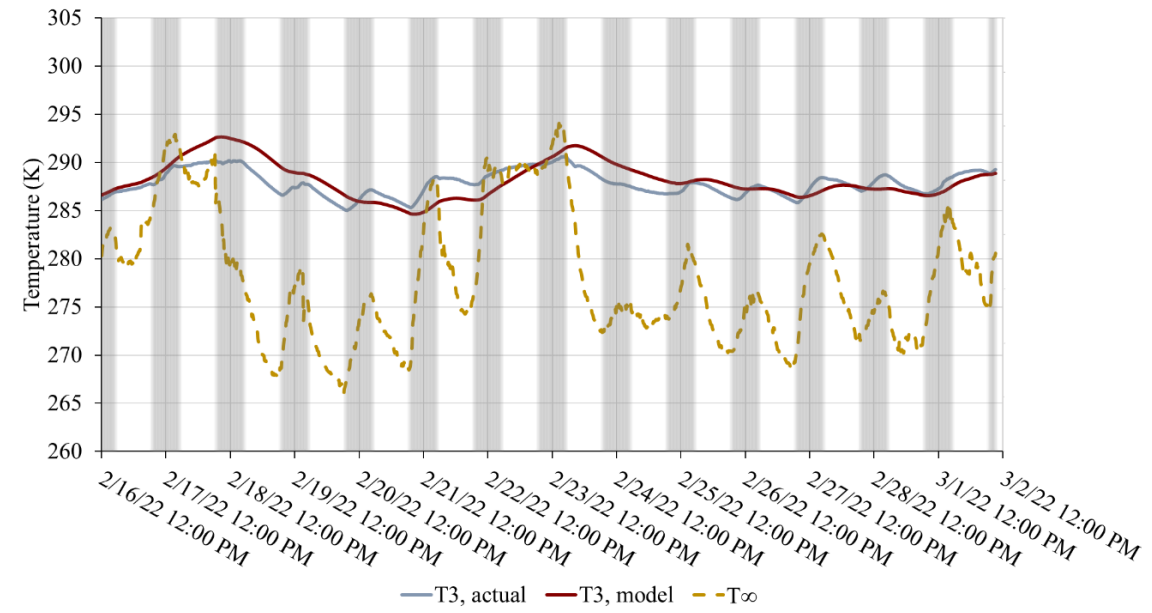

Figure 5.24

Modeled Temperature for Zone 4

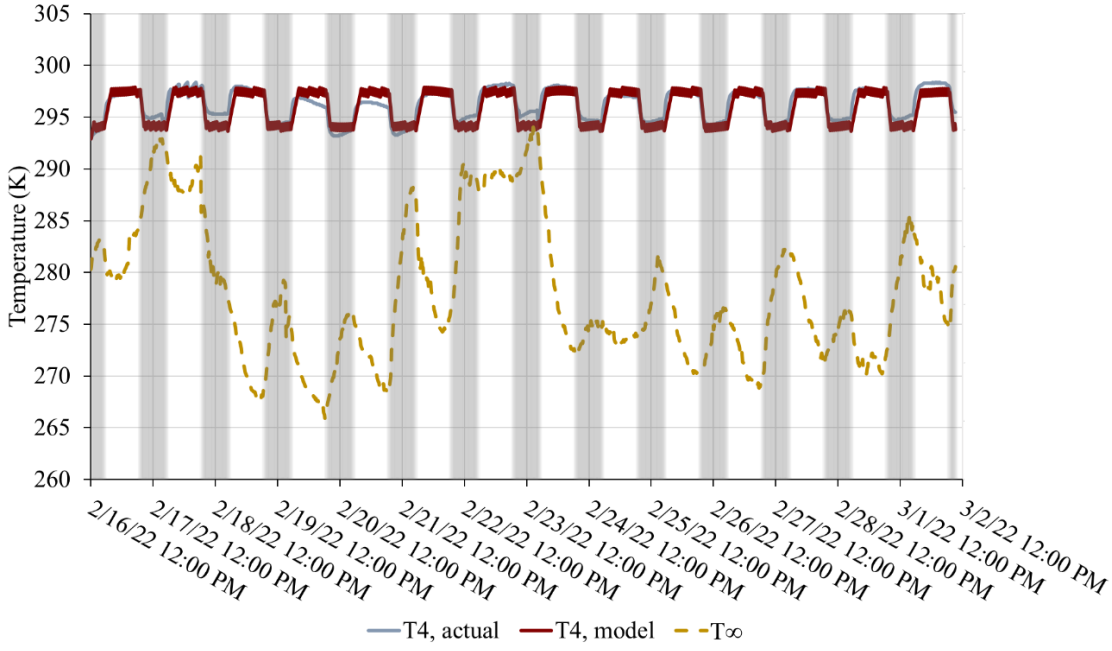

Figure 5.25

Modeled Temperature for Zone 5

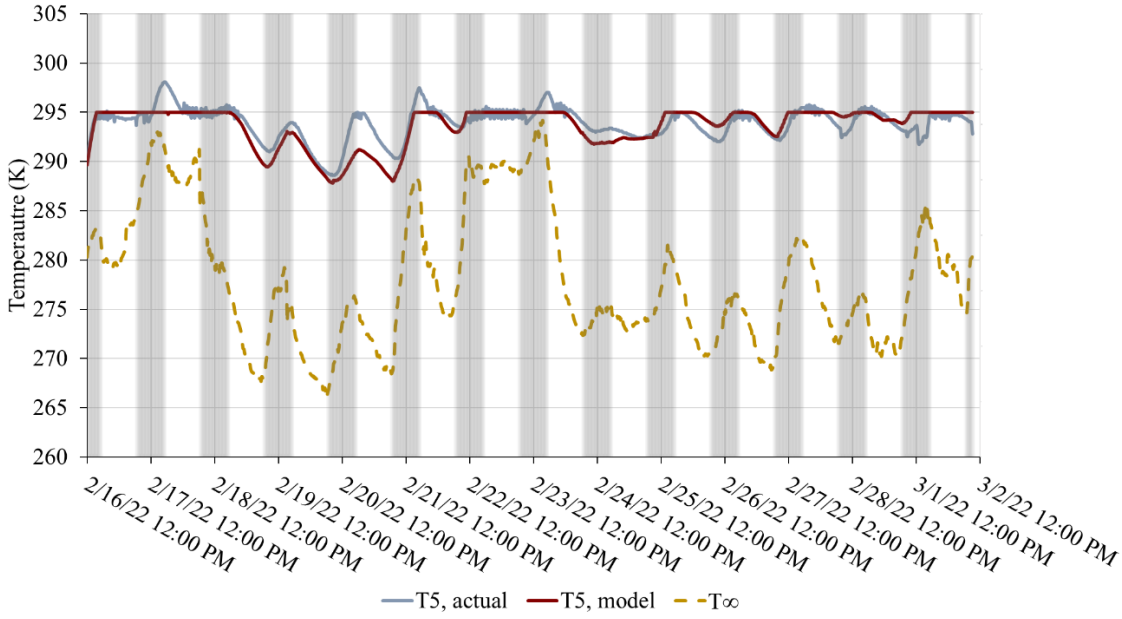

Table 5.4 displays the RMSE values for the average indoor zonal temperatures for different zones within Building B. The RMSE values calculated for Building B were found to be of similar magnitude to the temperature drift and ramp limits specified by AHSRAE (e.g., a monotonic change of 2.2 K over 1 hour) [119]. Although a direct mathematical comparison between the ASHRAE limits and RMSE values is not feasible, both metric are comparable in assessing deviations from the baseline temperature.

Table 5.4

RMSE Values for Average Indoor Zonal Temperatures in Building B

Zone	RMSE (K)
Zone 1	0.86
Zone 2	1.82
Zone 3	1.40
Zone 4	0.81
Zone 5	1.19

After confirming the model's accuracy, temperature setbacks were incorportated to evaluate potential financial and economic benefits. Initially, the model predicted that Building B consumed 1,680 kWh of energy during the specified data collection period. However, upon implementing temperatures setbacks, the energy consumption notably decreased to 1,562 kWh, resulting in savings of 7.0%.

Chapter 6

Conclusion

This research examines the impact of temperature setbacks implemented during an existing building's unoccupied hours in the heating season, with a particular focus on existing buildings maintained by the New Jersey Department of Military and Veterans Affairs. This investigation aligns with federal and state energy initiatives to reduce building energy consumption as detailed in TAG Policy Letter 18-5, Executive Order 13990, and the Energy Independence and Security Act of 2007 [9-12]. Therefore, three distinct categories of energy modeling were explored: white-box, black-box, and grey-box modeling, highlighting the unique advantages and inherent limitations associated with each modeling technique when modeling the energy consumption patterns of existing architectural structures.

Physics-based white-box models, such as eQUEST models based on the DOE-2 engine [14], can pose challenges when used for energy modeling in existing buildings. The inherent complexity of these models highlights the importance of possessing an in-depth understanding of the building's characteristics and the intricacies of the software both necessary to construct an eQUEST model accurately. This complexity arises from the necessity to encompass a vast array of building parameters, as presented in Table 5.1, as well as engage in multiple iterative calibration processes.

Furthermore, users with limited software experience may find it daunting to navigate the diverse array of user screens and settings within the software interface. Consequently, eQUEST may be better suited for energy modeling in new buildings, where parameters can be strategically chosen during the design phase. This approach

offers greater flexibility and control over the modeling process, ensuring that the model aligns effectively with the intended design and operational parameters of the new building.

Statistical black-box models, such as degree-day models, offer an efficient and straightforward approach to energy modeling. At their core, these models aim to establish a simple (often linear) relationship between degree-days and energy consumption, making them particularly accessible for analysis by non-experts. However, their utility is intrinsically tied to the consistency of a building's operational patterns. In essence, if there are significant shifts or alterations in how the building operates, maintaining the accuracy of this relationship may prove more challenging. Compared to white-box models, the degree-day approach may be a more pragmatic choice for comparing similar buildings and discerning shifts in building performance.

However, the degree-day model's effectiveness hinges on the availability of its own extensive data inputs, including local weather information and utility consumption data. These data sources are integral to the model's capacity to make accurate predictions regarding energy consumption and performance. In the absence of sufficient data availability, the degree-day model may not be a practical choice for energy modeling, underscoring the importance of data accessibility when considering this modeling approach.

Hybrid grey-box models, such as resistance-capacitance models, present a versatile and highly customizable method for energy modeling in existing buildings, offering a valuable tool for energy analysis and optimization. One notable feature of these models is their adaptability, allowing users to tailor the model's intricacy by adjusting the

number of resistive and capacitive elements in the model. However, this flexibility should be exercised with care, as more complex buildings often demand more intricate models, potentially increasing the modeling workload and necessary user expertise.

In addition to their flexibility, resistance-capacitance models are data-intensive, relying on a comprehensive dataset for accurate modeling. Key data inputs include indoor and outdoor temperature information, as well as utility consumption data. These inputs are crucial for the resistance-capacitance model to generate reliable predictions and insights regarding energy consumption and performance, making data availability a pivotal consideration when employing this modeling approach.

In conclusion, the selection of a modeling approach should be driven by the unique demands of the project, the accessibility of pertinent data, and the degree of precision desired. An understanding of the advantages and limitations inherent in each approach empowers researchers and building operators to make informed decisions, ensuring the selection of the most fitting methodology for conducting energy analyses and efficiency evaluations in diverse building contexts. It is crucial to recognize that no single modeling approach fits all scenarios; instead, a well-informed choice should align with the specific objectives and conditions of the project. Whether opting for a statistical black-box model, a physical white-box model, or a hybrid grey-box model, the suitability of the chosen approach hinges on its capacity to accurately capture and analyze the complexities of the building's physical, thermodynamic, and operational characteristics. Therefore, an understanding of these modeling techniques equips decision-makers with the tools needed to advance energy efficiency and sustainability goals within buildings.

6.1 Recommendations

The recommendations presented below, stemming from the insights gained through this research, are intended for the consideration of the client, the New Jersey Department of Military and Veterans Affairs (NJDMAVA). However, it is crucial to emphasize that these recommendations possess applicability beyond this specific client and context described in preceding chapter may benefit any building operator.

Fundamentally, data, as demonstrated in this research, plays a pivotal role in all varieties of energy models and stands as the foundation of knowledge acquisition. In simpler terms, possessing a thorough understanding of a building translates into an enhanced insight into how it operates, allowing the building operator to better optimize its efficiency. Data enriches the utility of energy models, fostering greater confidence in energy and cost saving forecasts. To facilitate this notion, the adoption of specific practices can substantially enhance a building operator's command over and comprehension of their building's operations.

For instance, the practice of documenting building alterations through a work order system or installing a building automation system can yield substantial benefits. These measures empower building operators by offering a more transparent view of how the building operates in response to various changes. In this context, smart meter data, a prevalent utility data storage system, plays a pivotal role. It provides direct insights into how a building consumes energy, essentially revealing how the building responds to alterations in its environment and weather conditions.

Finally, one of many key practices for building operators to consider is the implementation of temperature setbacks during unoccupied periods. Over conditioning a

building when it is essentially vacant constitutes an unnecessary expenditure of resources and counters current federal and state energy reduction initiatives, particularly within the military sector. Additionally, by curbing energy consumption, operating funds may be reallocated to other projects, ultimately enhancing the overall functionality of a building.

6.2 Future Work

While this research has provided valuable insights into energy modeling for existing buildings, there remain several avenues for future research and development. In this thesis, degree-day models were used to identify potential *historical* operational changes in the building. Considering additional work presented here for RC models in which effects of operational changes were *predicted*, the question arises: Can degree-day models be adapted similarly to the RC model to account for temperature setbacks during unoccupied hours?

Furthermore, this research uncovered limitations in the existing methodology for local temperature collection with HOBO meters (e.g., discussion in Section 4.3), highlighting the importance of importance of selecting the acquisition interval based on the building's (estimated) thermal time constant. For instance, in modeling the heater input in Building A, a numerical "noise" artifact was evident in the RC model due to the data acquisition interval exceeding the thermal time constant. Essentially, when the heater was activated, the model reflected a 15-minute activation period, which was excessive for Building A given its specific thermal time constant.

Finally, another crucial focus area is the development of a comparable RC model applicable during the cooling season, as the current assessment of Building B was limited to two weeks during the heating season. Ideally, full-year RC models would provide a

more precise understanding of the building's annual operations, enabling more accurate predictions of energy consumption and associated cost savings.

References

[1] LLNL. "United States Energy Flow Chart, 2019." Lawrence Livermore National Laboratory. https://flowcharts.llnl.gov/commodities/energy (accessed 2021).

[2] IEA. "Key World Energy Statistics 2021." https://www.iea.org/reports/key-world-energy-statistics-2021 (accessed 2021).

[3] M. Denchak. "Fossil Fuels: The Dirty Facts." Natural Resources Defense Council. https://www.nrdc.org/stories/fossil-fuels-dirty-facts (accessed 2021).

[4] H. Ritchie, P. Rosado, and M. Roser, "Energy," *Our World in Data*, 2022. [Online]. Available: https://ourworldindata.org/energy.

[5] O. Kaze. "EIA expects U.S. fossil fuels productions to reach new highs in 2023." United States Energy Information Administration. https://www.eia.gov/todayinenergy/detail.php?id=50978#:~:text=EIA%20expects%20U.S.%20fossil%20fuel%20production%20to%20reach%20new%20highs%20in%202023&text=After%20declining%20in%202020%2C%20the,77.14%20quadrillion%20British%20thermal%20units. (accessed 2021).

[6] AIA. "Joining the 2030 Commitment: What to expect." American Institute of Architects. (accessed 2021).

[7] A. Guterres. "Carbon neutrality by 2050: the world's most urgent mission." United Nations. https://www.un.org/sg/en/content/sg/articles/2020-12-11/carbon-neutrality-2050-the-world%E2%80%99s-most-urgent-mission (accessed 2021).

[8] P. Towell and L. M. Williams, "Defense: FY2017 Budget Request, Authorization, and Appropriation," Congressional Research Service, 2017. [Online]. Available: https://sgp.fas.org/crs/natsec/R44454.pdf

[9] (2019). *TAG Policy Letter 18-5*.

[10] (2021). *Executive Order 139890: Protecting the Public Health and the Environment and Restoring Science to Tackle the Climate Crisis*. [Online] Available: https://www.govinfo.gov/content/pkg/FR-2021-01-25/pdf/2021-01765.pdf

[11] (2007). *Energy Independence and Security Act of 2007*. [Online] Available: https://www.govinfo.gov/content/pkg/BILLS-110hr6enr/pdf/BILLS-110hr6enr.pdf

[12] (2019). *2019 New Jersey Energy Master Plan: Pathway to 2050*. [Online] Available: http://d31hzlhk6di2h5.cloudfront.net/20200127/84/84/03/b2/2293766d081ff4a3cd8e60aa/NJBPU_EMP.pdf

[13] D. A. Roth. "Building Energy Modeling." United States Department of Energy. https://www.energy.gov/eere/buildings/building-energy-modeling (accessed 2023).

[14] J. J. Hirsch. "eQUEST: the QUick Energy Simulation Tool." https://www.doe2.com/equest/ (accessed 2021).

[15] C. DeKorne, "Heat Transfer Through Buildings," *Journal of Light Construction*, no. July, pp. 5-7, 07/2019 2019.

[16] USEPA. "ENERGY STAR Certified Homes Building Science Information." United States Environmental Protection Agency. https://www.energystar.gov/ia/partners/bldrs_lenders_raters/downloads/ENERGY_STAR_V3_Building_Science.pdf?d387-4a5e= (accessed 2021).

[17] UWSP. "Unite 2: Energy Rules!" University of Wisconsin Stevens Point. https://www3.uwsp.edu/cnr-ap/KEEP/nres633/Pages/Unit2/Section-A-Introduction.aspx (accessed 2021).

[18] J. Leckie, G. Masters, H. Whitehouse, and L. Young, *More Other Homes and Garbage: Designs for Self-Sufficient Living*. Sierra Club, 1981.

[19] D. M. Bahrami, "Steady Condution Heat Transfer," Simon Fraser University, 2011. [Online]. Available: https://www.sfu.ca/~mbahrami/ENSC%20388/Notes/Staedy%20Conduction%20Heat%20Transfer.pdf

[20] X. Dérobert, J.-P. Balayssac, Z. M. Sbartaï, and J. Dumoulin, "3 - Electromagnetic Methods," in *Non-Destructive Testing and Evaluation of Civil Engineering Structures*, J.-P. Balayssac and V. Garnier Eds.: Elsevier, 2018, pp. 87-137.

[21] EERE. "Solar Radiation Basics." Office of Energy Efficiency & Renewable Energy. https://www.energy.gov/eere/solar/solar-radiation-basics (accessed 3/23/2023.

[22] NASA. "Solar Irradiance." National Aeronautics and Space Administration. https://www.energy.gov/eere/solar/solar-radiation-basics (accessed 3/23/2023, 2023).

[23] H. Zhang, F. Che, T. Lin, and W. Zhao, "3 - Thermal modeling, analysis, and design," in *Modeling, Analysis, Design, and Tests for Electronics Packaging beyond Moore*, H. Zhang, F. Che, T. Lin, and W. Zhao Eds.: Woodhead Publishing, 2020, pp. 59-129.

[24] NPL. "What is emissivity and why is it important?" National Physics Laboratory. https://www.npl.co.uk/resources/q-a/why-is-emissivity-important (accessed 2021).

[25] S. Taylor, J. B. Wright, E. C. Forrest, B. Jared, J. Koepke, and J. Beaman, "Investigating relationship between surface topography and emissivity of metallic additively manufactured parts," *International Communications in Heat and Mass Transfer*, vol. 115, p. 104614, 2020/06/01/ 2020, doi: https://doi.org/10.1016/j.icheatmasstransfer.2020.104614.

[26] R. M. S. F. A. Eva Barreira, Maria L. Simões, "Emissivity of Building Materials for Infrared Measurements," 03/11/2021 2021, doi: https://doi.org/10.3390%2Fs21061961.

[27] DOE. "Basic Principles of Heat Transfer." Department of Energy. https://bsesc.energy.gov/training-modules/heat-transfer (accessed 2021).

[28] I. Koren and C. M. Krishna, "Temperature-aware computing," *Sustainable Computing: Informatics and Systems*, vol. 1, no. 1, pp. 46-56, 2011/03/01/ 2011, doi: https://doi.org/10.1016/j.suscom.2010.10.004.

[29] D. Kosiachevskyi, M. Babenko, M. Savytskyi, M. Schmidt, and I. Pereginets, "The main insulation parameters for the design of NZEB from biosourced materials," *Construction Materials Science Mechanical Engineering*, p. 7, 04/25 2017. [Online]. Available: https://www.researchgate.net/publication/349443826_The_main_insulation_parameters_for_the_design_of_NZEB_from_biosourced_materials.

[30] A. E. Saied, C. Maalouf, T. Bejat, and E. Wurtz, "Slab-on-grade thermal bridges: A thermal behavior and solution review," *Energy and Buildings*, vol. 257, p. 111770, 2022/02/15/ 2022, doi: https://doi.org/10.1016/j.enbuild.2021.111770.

[31] ASHRAE, *ASHRAE Handbook of Fundamentals*. The American Society of Heating, Refrigerating, and Air-Conditioning Engineers, 2022.

[32] USDOE. "Ventilation." United States Department of Energy. https://www.energy.gov/energysaver/ventilation (accessed 2023).

[33] USEPA. "An Office Building Occupant's Guide to Indoor Air Quality." United States Environmental Protection Agency. https://www.epa.gov/indoor-air-quality-iaq/indoor-air-quality-offices-and-other-large-buildings (accessed 2022).

[34] V. C. Thomas. "Ventilation, Infiltration, and Exfiltration." Energy-Models. https://energy-models.com/ventilation-infiltration-exfiltration (accessed 2023).

[35] M. H. Sherman, "Tracer-gas techniques for measuring ventilation in a single zone," *Building and Environment*, vol. 25, no. 4, pp. 365-374, 1990/01/01/ 1990, doi: https://doi.org/10.1016/0360-1323(90)90010-O.

[36] A. A. Chowdhury, M. G. Rasul, and M. M. K. Khan, "Thermal performance assessment of a retrofitted building using an integrated energy and computational fluid dynamics (IE - CFD) approach," *Energy Reports*, vol. 8, pp. 709-717, 2022/12/01/ 2022, doi: https://doi.org/10.1016/j.egyr.2022.10.365.

[37] USDOE. "Continuous Air Barrier in Exterior Walls." United States Department of Energy. https://basc.pnnl.gov/resource-guides/continuous-air-barrier-exterior-walls#:~:text=The%20home's%20thermal%20barrier%20of,compressions%2C%20gaps%2C%20or%20voids. (accessed 2023).

[38] W. A. Steven J. Emmerich; Timothy P. McDowell, "Investigation of the Impact of Commercial Building Envelope Airtightnesss on HVAC Energy Use," 2005. [Online]. Available: https://www.nist.gov/publications/investigation-impact-commercial-building-envelope-airtightness-hvac-energy-use-0

[39] X. Zheng, E. W. Cooper, J. Mazzon, I. Wallis, and C. J. Wood, "Experimental insights into the airtightness measurement of a house-sized chamber in a sheltered environment using blower door and pulse methods," *Building and Environment*, vol. 162, p. 106269, 2019/09/01/ 2019, doi: https://doi.org/10.1016/j.buildenv.2019.106269.

[40] Y. Ji and L. Duanmu, "Airtightness field tests of residential buildings in Dalian, China," *Building and Environment*, vol. 119, pp. 20-30, 2017/07/01/ 2017, doi: https://doi.org/10.1016/j.buildenv.2017.03.043.

[41] USDOE. "Solar Radiation Basics." United States Department of Energy. https://www.energy.gov/eere/solar/solar-radiation-basics (accessed 2023).

[42] NASA. "The Earth's Radiation Budget." https://science.nasa.gov/ems/13_radiationbudget#:~:text=Incoming%20ultraviolet%2C%20visible%2C%20and%20a,drive%20the%20Earth's%20climate%20system. (accessed 2022).

[43] NASA. "Data Products: Downward Shortwave Radiation (Surface)." National Oceanic and Atmospheric Administration; National Aeronautics and Space Administration. https://www.goes-r.gov/products/baseline-DSR.html#:~:text=The%20downward%20shortwave%20radiation%20(DSR,that%20reaches%20the%20Earth's%20surface. (accessed 2022).

[44] NREL. "Solar Resource Maps and Data." The National Renewable Energy Laboratory. https://www.nrel.gov/gis/solar-resource-maps.html (accessed 2022).

[45] NASA. POWER Data Access Viewer [Online] Available: https://power.larc.nasa.gov/data-access-viewer/

[46] Gigahertz-Optik. "Reflection, Transmission, and Absorption." Gigahertz-Optik. https://light-measurement.com/reflection-absorption/#:~:text=Reflection%2C%20transmission%20and%20scattering%20leave,heat%2C%20by%20interaction%20with%20matter. (accessed 2023).

[47] H. Li, H. Jia, K. Zhong, and Z. Zhai, "Analysis of factors influencing actual absorption of solar energy by building walls," *Energy*, vol. 215, p. 118988, 2021/01/15/ 2021, doi: https://doi.org/10.1016/j.energy.2020.118988.

[48] F. Babota, D. Manea, C. Aciu, R. Iernutan, and L. Molnar, *Shading - the way for solar control and reduction of heat gain in buildings*. 2013.

[49] ETB. "Radiation Heat Transfer." The Engineering ToolBox. https://www.engineeringtoolbox.com/radiation-heat-transfer-d_431.html#:~:text=Heat%20transfer%20due%20to%20emission,is%20known%20as%20thermal%20radiation.&text=Heat%20transfer%20through%20radiation%20takes,agitation%20of%20its%20composing%20molecules. (accessed.

[50] Anonymous. "Heating, Ventilation and Air-Conditioning Systems, Part of Indoor Air Quality Design Tools for Schools." United States Environmental Protection Agency. https://www.epa.gov/iaq-schools/heating-ventilation-and-air-conditioning-systems-part-indoor-air-quality-design-tools (accessed 06/09/2023, 2023).

[51] M. Mourshed, "Relationship between annual mean temperature and degree-days," *Energy and Buildings,* vol. 54, pp. 418-425, 2012/11/01/ 2012, doi: https://doi.org/10.1016/j.enbuild.2012.07.024.

[52] T. Day, *Degree-days: theory and application*. The Chartered Institution of Building Services Engineers, 2006.

[53] S. Lu, W. Wang, C. Lin, and E. C. Hameen, "Data-driven simulation of a thermal comfort-based temperature set-point control with ASHRAE RP884," *Building and Environment,* vol. 156, pp. 137-146, 2019/06/01/ 2019, doi: https://doi.org/10.1016/j.buildenv.2019.03.010.

[54] EIA. "Units and calculators explained: Degree days." United States Energy Information Agency. https://www.eia.gov/energyexplained/units-and-calculators/degree-days.php (accessed 2023).

[55] EERE, "About Building Energy Modeling," 2022. [Online]. Available: https://www.energy.gov/eere/buildings/about-building-energy-modeling#:~:text=Building%20Energy%20Modeling%20(BEM)%20is%20a%20multi%2Dpurpose%20tool,(program%20development%2C%20research).

[56] D. Goldwasser. "Building Energy Modeling." National Renewable Energy Laboratory. (accessed 2023).

[57] K. Cleary and K. Palmer. "Energy Efficiency 101." Resources for the Future 70. https://www.rff.org/publications/explainers/energy-efficiency-101/#:~:text=Energy%20efficiency%20refers%20to%20using,to%2080%20percent%20less%20electricity. (accessed 2023).

[58] K. Amasyali and N. M. El-Gohary, "A review of data-driven building energy consumption prediction studies," *Renewable and Sustainable Energy Reviews,* vol. 81, pp. 1192-1205, 2018/01/01/ 2018, doi: https://doi.org/10.1016/j.rser.2017.04.095.

[59] A. Duun-Henriksen *et al.*, "Model Identification Using Stochastic Differential Equation Grey-Box Models in Diabetes," *Journal of diabetes science and technology,* vol. 7, pp. 431-440, 03/01 2013, doi: 10.1177/193229681300700220.

[60] F. Amara, K. Agbossou, A. Cardenas, Y. Dubé, and S. Kelouwani, "Comparison and Simulation of Building Thermal Models for Effective Energy Management," *Smart Grid and Renewable Energy,* vol. 06, pp. 95-112, 01/01 2015, doi: 10.4236/sgre.2015.64009.

[61] Autodesk. "Cloud-based energy simulation." Autodesk. https://gbs.autodesk.com/gbs (accessed 2022).

[62] A. Roth. "EnergyPlus." EnergyPlus. https://energyplus.net/ (accessed 2023).

[63] TRNSYS. "Applications." https://www.trnsys.com/#2 (accessed 2023).

[64] Autodesk. "Revit: BIM software for designers, builders, and doers." Autodesk. https://www.autodesk.com/products/revit/overview?term=1-YEAR&tab=subscription (accessed 2023).

[65] N. Mostafavi, M. Farzinmoghadam, and S. Hoque, "Envelope retrofit analysis using eQUEST, IESVE, Revit Plug-in, and Green Building Studio: a university dormitory case study," *International Journal of Sustainable Energy,* vol. 34, no. 9, pp. 594-613, 2013. [Online]. Available: https://www.tandfonline.com/doi/citedby/10.1080/14786451.2013.848207?scroll=top&needAccess=true&role=tab.

[66] H. S. Rallapalli, "A Comparison of EnergyPlus and eQUEST Whole Building Energy Simulation Results for a Medium Sized Office Building," 2010. [Online]. Available: https://keep.lib.asu.edu/_flysystem/fedora/c7/29477/Rallapalli_asu_0010N_10220.pdf

[67] A. Dutta and A. Samanta, "Reducing cooling load of buildings in the tropical climate through window glazing: A model to model comparison," *Journal of Building Engineering,* vol. 15, pp. 318-327, 2018/01/01/ 2018, doi: https://doi.org/10.1016/j.jobe.2017.12.005.

[68] J. Song, X. Zhang, and X. Meng, "Simulation and Analysis of a University Library Energy Consumption based on EQUEST," *Procedia Engineering,* vol. 121, pp. 1382-1388, 2015/01/01/ 2015, doi: https://doi.org/10.1016/j.proeng.2015.09.028.

[69] A. Zerroug and E. Dzelzitis, "Analysis of different building exterior walls insulations using eQUEST," *E3S Web of Conferences,* vol. 111, p. 06032, 01/01 2019, doi: 10.1051/e3sconf/201911106032.

[70] M. Zafaranchi, "Simulation and Analysis of Passive Parameters of Building in eQuest: A Case Study in Istanbul, Turkey," *Engineering and Technology*

International Journal of Energy and Environmental Engineering, vol. 14, 2020. [Online]. Available: https://publications.waset.org/10011481/simulation-and-analysis-of-passive-parameters-of-building-in-equest-a-case-study-in-istanbul-turkey.

[71] M.-T. Ke, C.-H. Yeh, and J.-T. Jian, "Analysis of building energy consumption parameters and energy savings measurement and verification by applying eQUEST software," *Energy and Buildings,* vol. 61, pp. 100-107, 2013/06/01/ 2013, doi: https://doi.org/10.1016/j.enbuild.2013.02.012.

[72] H. M. Teamah, A. E. Kabeel, and M. Teamah, "Potential retrofits in office buildings located in harsh Northern climate for better energy efficiency, cost effectiveness, and environmental impact," *Process Safety and Environmental Protection,* vol. 162, pp. 124-133, 2022/06/01/ 2022, doi: https://doi.org/10.1016/j.psep.2022.03.067.

[73] A. Muhammad and S. Karinka, "Comparative energy analysis of a laboratory building with different materials using eQUEST simulation software," *Materials Today: Proceedings,* vol. 52, pp. 2160-2165, 2022/01/01/ 2022, doi: https://doi.org/10.1016/j.matpr.2022.01.187.

[74] J. Xing, P. Ren, and J. Ling, "Analysis of energy efficiency retrofit scheme for hotel buildings using eQuest software: A case study from Tianjin, China," *Energy and Buildings,* vol. 87, pp. 14-24, 2015/01/01/ 2015, doi: https://doi.org/10.1016/j.enbuild.2014.10.045.

[75] C. Leung and H. Ge, "Sleep thermal comfort and the energy saving potential due to reduced indoor operative temperature during sleep," *Building and Environment,* vol. 59, pp. 91-98, 2013/01/01/ 2013, doi: https://doi.org/10.1016/j.buildenv.2012.08.010.

[76] M. Y. Khan and A. Baqi, "Experimental and theoretical analysis of a new kind of building envelope," *Materials Today: Proceedings,* vol. 43, pp. 1368-1375, 2021/01/01/ 2021, doi: https://doi.org/10.1016/j.matpr.2020.09.171.

[77] X. Li and J. Wen, "Review of building energy modeling for control and operation," *Renewable and Sustainable Energy Reviews,* vol. 37, pp. 517-537, 2014/09/01/ 2014, doi: https://doi.org/10.1016/j.rser.2014.05.056.

[78] X. Li, J. Wen, and E. Bai, *Building energy forecasting using system identification based on system characteristics test*. 2015.

[79] N. Fumo and M. A. Rafe Biswas, "Regression analysis for prediction of residential energy consumption," *Renewable and Sustainable Energy Reviews,* vol. 47, pp. 332-343, 2015/07/01/ 2015, doi: https://doi.org/10.1016/j.rser.2015.03.035.

[80] M. R. Braun, H. Altan, and S. B. M. Beck, "Using regression analysis to predict the future energy consumption of a supermarket in the UK," *Applied Energy,* vol. 130, pp. 305-313, 2014/10/01/ 2014, doi: https://doi.org/10.1016/j.apenergy.2014.05.062.

[81] A. Aranda, G. Ferreira, M. D. Mainar-Toledo, S. Scarpellini, and E. Llera Sastresa, "Multiple regression models to predict the annual energy consumption in the Spanish banking sector," *Energy and Buildings,* vol. 49, pp. 380-387, 2012/06/01/ 2012, doi: https://doi.org/10.1016/j.enbuild.2012.02.040.

[82] F. S. Mosonye, "Production, Energy Consumption and Simple Linear Regression: A Though Experiment," ed, 2019.

[83] P. Zhang, "Chapter 19 - Industrial control system simulation routines," in *Advanced Industrial Control Technology*, P. Zhang Ed. Oxford: William Andrew Publishing, 2010, pp. 781-810.

[84] B. Omarov, S. A. Memon, and J. Kim, "A novel approach to develop climate classification based on degree days and building energy performance," *Energy*, vol. 267, p. 126514, 2023/03/15/ 2023, doi: https://doi.org/10.1016/j.energy.2022.126514.

[85] S. Abebe and T. Assefa, "Development of climatic zoning and energy demand prediction for Ethiopian cities in degree days," *Energy and Buildings*, vol. 260, p. 111935, 2022/04/01/ 2022, doi: https://doi.org/10.1016/j.enbuild.2022.111935.

[86] G. Martinopoulos, A. Alexandru, and K. T. Papakostas, "Mapping temperature variation and degree-days in metropolitan areas with publicly available sensors," *Urban Climate*, vol. 28, p. 100464, 2019/06/01/ 2019, doi: https://doi.org/10.1016/j.uclim.2019.100464.

[87] A. Matzarakis and C. Balafoutis, "Heating degree-days over Greece as an index of energy consumption," *International Journal of Climatology*, https://doi.org/10.1002/joc.1107 vol. 24, no. 14, pp. 1817-1828, 2004/11/30 2004, doi: https://doi.org/10.1002/joc.1107.

[88] Z. Shiqiang and Z. Xiaowen, "Evaluation of glacier runoff in Tailan basin by monthly degree-day model," in *2009 IEEE International Geoscience and Remote Sensing Symposium*, 12-17 July 2009 2009, vol. 2, pp. II-582-II-585, doi: 10.1109/IGARSS.2009.5418151.

[89] Q. You *et al.*, "Present and projected degree days in China from observation, reanalysis and simulations," *Climate Dynamics*, vol. 43, no. 5, pp. 1449-1462, 2014/09/01 2014, doi: 10.1007/s00382-013-1960-0.

[90] M. Safa, B. Kc, and M. Safa, "Linear Model to Predict Energy Consumption Using Historical Data From Cold Stores," 2015. [Online]. Available: https://core.ac.uk/download/pdf/92972692.pdf

[91] P. P. Moletsane, T. J. Motlhamme, R. Malekian, and D. C. Bogatmoska, "Linear regression analysis of energy consumption data for smart homes," in *2018 41st International Convention on Information and Communication Technology, Electronics and Microelectronics (MIPRO)*, 21-25 May 2018 2018, pp. 0395-0399, doi: 10.23919/MIPRO.2018.8400075.

[92] A. M. R. Nishimwe and S. Reiter, "Using artificial intelligence models and degree-days method to estimate the heat consumption evolution of a building stock until 2050: A case study in a temperate climate of the Northern part of Europe," *Cleaner and Responsible Consumption*, vol. 5, p. 100069, 2022/06/01/ 2022, doi: https://doi.org/10.1016/j.clrc.2022.100069.

[93] J. Terés-Zubiaga, E. Pérez-Iribarren, I. González-Pino, and J. M. Sala, "Effects of individual metering and charging of heating and domestic hot water on energy consumption of buildings in temperate climates," *Energy Conversion and Management*, vol. 171, pp. 491-506, 2018/09/01/ 2018, doi: https://doi.org/10.1016/j.enconman.2018.06.013.

[94] L. M. Al-Hadhrami, "Comprehensive review of cooling and heating degree days characteristics over Kingdom of Saudi Arabia," *Renewable and Sustainable Energy Reviews*, vol. 27, pp. 305-314, 2013/11/01/ 2013, doi: https://doi.org/10.1016/j.rser.2013.04.034.

[95] D. Zivar, A. Ishanov, and P. Pourafshary, "Insights into wettability alteration during low-salinity water flooding by capacitance-resistance model," *Petroleum Research*, 2022/01/17/ 2022, doi: https://doi.org/10.1016/j.ptlrs.2022.01.004.

[96] O. I. O. Ogali and O. D. Orodu, "Fault characterization and flow barrier detection using capacitance-resistance model and diagnostic plots," *Journal of Petroleum Science and Engineering*, vol. 209, p. 109817, 2022/02/01/ 2022, doi: https://doi.org/10.1016/j.petrol.2021.109817.

[97] J. A. Al-Sudani, H. K. Mustafa, D. F. Al-Sudani, and H. Falih, "Analytical water saturation model using capacitance-resistance simulation: Clean and shaly formations," *Journal of Natural Gas Science and Engineering*, vol. 82, p. 103325, 2020/10/01/ 2020, doi: https://doi.org/10.1016/j.jngse.2020.103325.

[98] A. Mamghaderi, B. Aminshahidy, and H. Bazargan, "Prediction of waterflood performance using a modified capacitance-resistance model: A proxy with a time-correlated model error," *Journal of Petroleum Science and Engineering*, vol. 198, p. 108152, 2021/03/01/ 2021, doi: https://doi.org/10.1016/j.petrol.2020.108152.

[99] R. Wanderley de Holanda, E. Gildin, and J. L. Jensen, "A generalized framework for Capacitance Resistance Models and a comparison with streamline allocation factors," *Journal of Petroleum Science and Engineering*, vol. 162, pp. 260-282, 2018/03/01/ 2018, doi: https://doi.org/10.1016/j.petrol.2017.10.020.

[100] G. A. Moreno, "Multilayer capacitance–resistance model with dynamic connectivities," *Journal of Petroleum Science and Engineering,* vol. 109, pp. 298-307, 2013/09/01/ 2013, doi: https://doi.org/10.1016/j.petrol.2013.08.009.

[101] M. Sayarpour, E. Zuluaga, C. S. Kabir, and L. W. Lake, "The use of capacitance–resistance models for rapid estimation of waterflood performance and optimization," *Journal of Petroleum Science and Engineering,* vol. 69, no. 3, pp. 227-238, 2009/12/01/ 2009, doi: https://doi.org/10.1016/j.petrol.2009.09.006.

[102] Z. Tong, H. Wu, Y. Guan, Y. Ji, and S. Hu, "Resistance-capacitance model of the capillary heat exchanger in subway tunnels," *Energy and Built Environment,* 2022/07/06/ 2022, doi: https://doi.org/10.1016/j.enbenv.2022.07.002.

[103] H. R. Liu, L. J. Hua, B. J. Li, C. X. Wang, and R. Z. Wang, "Thermal resistance-capacitance network model for fast simulation on the desiccant coated devices used for effective electronic cooling," *International Journal of Refrigeration,* vol. 131, pp. 78-86, 2021/11/01/ 2021, doi: https://doi.org/10.1016/j.ijrefrig.2021.07.038.

[104] A. Najib, A. Zarrella, V. Narayanan, P. Grant, and C. Harrington, "A revised capacitance resistance model for large diameter shallow bore ground heat exchanger," *Applied Thermal Engineering,* vol. 162, p. 114305, 2019/11/05/ 2019, doi: https://doi.org/10.1016/j.applthermaleng.2019.114305.

[105] H. Wan, X. Xu, T. Xu, K. K. R. Yuen, and G. Huang, "Development of a quasi-2D variable resistance–capacitance model for tube-encapsulated phase change material storage tanks," *Applied Thermal Engineering,* vol. 214, p. 118868, 2022/09/01/ 2022, doi: https://doi.org/10.1016/j.applthermaleng.2022.118868.

[106] A. Jamali and A. Ettehadtavakkol, "Application of capacitance resistance models to determining interwell connectivity of large-scale mature oil fields," *Petroleum Exploration and Development,* vol. 44, no. 1, pp. 132-138, 2017/02/01/ 2017, doi: https://doi.org/10.1016/S1876-3804(17)30017-4.

[107] A. Li, Y. Sun, and X. Xu, "Development of a simplified resistance and capacitance (RC)-network model for pipe-embedded concrete radiant floors," *Energy and Buildings,* vol. 150, pp. 353-375, 2017/09/01/ 2017, doi: https://doi.org/10.1016/j.enbuild.2017.06.011.

[108] B.-K. Jeon, E.-J. Kim, Y. Shin, and K.-H. Lee, "Learning-Based Predictive Building Energy Model Using Weather Forecasts for Optimal Control of Domestic Energy Systems," *Sustainability*, vol. 11, no. 1, doi: 10.3390/su11010147.

[109] J. H. Kämpf and D. Robinson, "A simplified thermal model to support analysis of urban resource flows," *Energy and Buildings*, vol. 39, no. 4, pp. 445-453, 2007/04/01/ 2007, doi: https://doi.org/10.1016/j.enbuild.2006.09.002.

[110] ESP-r. "A Tour of ESP-r." ESP-r. https://www.esru.strath.ac.uk/Courseware/ESP-r/tour/ (accessed 2023).

[111] AvidXchange. UtilityAnalytics [Online] Available: https://utilityanalytics.avidxchange.net/

[112] Wyze. "Wyze Cam v3." https://www.wyze.com/products/wyze-cam?related_selling_plan=41618559008930 (accessed 2023).

[113] (2006). *Departmental Directive 25.2.3*. [Online] Available: https://www.nj.gov/military/publications/dd/DD25.2.3.pdf

[114] BizEE. "Degree Days Calculated Accurately for Locations Worldwide." BizEE. https://www.degreedays.net/ (accessed 2023).

[115] Onset. "The proof is in the data." Onset. https://www.onsetcomp.com/ (accessed 2023).

[116] USDOE. "Insulation." United States Department of Energy. https://www.energy.gov/energysaver/insulation (accessed 2023).

[117] Littlefuse. "Thermal Time Constant." Littelfuse. https://www.littelfuse.com/technical-resources/technical-centers/temperature-sensors/thermistor-info/thermistor-terminology/thermal-time-constant.aspx#:~:text=The%20Thermal%20Time%20Constant%20is,change%20in%20the%20ambient%20temperature. (accessed 2023).

[118] N. Mathur, I. Glesk, and A. Buis, "Thermal time constant: optimising the skin temperature predictive modelling in lower limb prostheses using Gaussian processes," *Healthcare Technology Letters,* https://doi.org/10.1049/htl.2015.0023 vol. 3, no. 2, pp. 98-104, 2016/06/01 2016, doi: https://doi.org/10.1049/htl.2015.0023.

[119] *ANSI/ASHRAE Standard 55-2004*, ASHRAE, 2004. [Online]. Available: http://arco-hvac.ir/wp-content/uploads/2015/11/ASHRAE_Thermal_Comfort_Standard.pdf

[120] (2008). *AR 420-1: Army Facilities Management*. [Online] Available: https://armypubs.army.mil/epubs/DR_pubs/DR_a/pdf/web/ARN15517_R420_1_admin_FINAL.pdf

[121] USEIA. "New Jersey State Energy Profile." United States Energy Information Association. https://www.eia.gov/state/print.php?sid=NJ (accessed 2023).

[122] USEPA. "Greenhouse Gases Equivalent Calculator - Calculations and References." United States Environmental Protection Agency. https://www.epa.gov/energy/greenhouse-gases-equivalencies-calculator-calculations-and-references (accessed 2023).

Appendix A

Additional Building Details of Building A

This appendix provides further information regarding Building A. Specifically, Table A.1 provides an overview of the surfaces within the 4R2C model for Building A, offering insights into their orientation, surface area, and neighboring spaces.

Table A.1

Surfaces in Building A

Surface	Orientation	Surface Area (m^2)	Adjacent Spaces	
Wall	Vertical	46.8	Lower Area	Outside
Window	Vertical	1.7	Lower Area	Outside
Door	Vertical	1.8	Lower Area	Outside
Lower Area Floor	Horizontal	14.8	Lower Area	Ground
Lower Area Ceiling	Horizontal	14.8	Lower Area	Upper Area
Roof	Sloped	35.5	Upper Area	Outside

Appendix B

Additional Building Details of Building B

This appendix provides further information regarding Building B. Specifically, Table B.1 provides an overview of the zonal surfaces within the 4R5C model for Building B, offering insights into their surface area and neighboring spaces. Additionally, Table B.2 provides a roster of rooms and their respective types.

Table B.1

Heat Loss Rate Variables for the 4R5C Model

	Ground	**Outside**	**1**	**2**	**3**	**4**	**5**
Ground	-	N/A	F (457 m^2)	F (363 m^2)	F (103 m^2)	F (9 m^2)	F (9 m^2)
Outside		-	R (457 m^2) EW (189 m^2)	R (363 m^2) EW (94 m^2)	R (103 m^2) EW (81 m^2)	R (9 m^2)	R (9 m^2) EW (8 m^2)
1			-	IW (49 m^2)	-	-	-
2				-	IW (31 m^2)	IW (16 m^2)	IW (9 m^2)
3					-	IW (9 m^2)	IW (9 m^2)
4						-	IW (8 m^2)
5							-

Symmetric

Note. Dimension of building component in parentheses.

Table B.2

Room Types at Building B

Room #	Room Type
100	Lobby
101	Office
102	Armorer's Office
103	Supply/Server Room
104	Boiler Room
105	Equipment Room
106	Electrical/Communications Room
107	Women's Room
108	Men's Room
109	Classroom/Conference Room
110	Caged Storage (Unheated)